Biodistribution and targeting properties of iron oxide nanoparticles for treatments of cancer and iron anemia disease

Edouard Alphandéry

Biodistribution and targeting properties of iron oxide nanoparticles for treatments of cancer and iron anemia disease

Edouard Alphandéry[+,*,++]

[+]Paris Sorbonne Université, Muséum National d'Histoire Naturelle, UMR CNRS 7590, IRD, Institut de Minéralogie, de Physique des Matériaux et de Cosmochimie, IMPMC, 75005 Paris, France

[*]Nanobacterie SARL, 36 boulevard Flandrin, 75116, Paris, France.

[++]Institute of Anatomy, UZH University of Zurich, Instiute of Anatomy, Winterthurerstrasse 190, CH-8057, Zurich, Switzerland.

Email address: edouardalphandery@hotmail.com, phone: 0033632697020

ABSTRACT: IONP commercialized for treatments of iron anemia or cancer diseases can be administered at doses exceeding 1 gram per patient, indicating their bio-compatibility when they are prepared in the right conditions. Various parameters influence IONP biodistribution such as nanoparticle size, hydrophobicity/hydrophilicity, surface charge, core composition, coating properties, route of administration, quantity administered, and opsonization. IONP biodistribution trends include their capture by the reticuloendothelial system (RES), accumulation in liver and spleen, leading to nanoparticle degradation by macrophages and liver Kupffer cells, possibly followed by excretion in feces. To result in efficient tumor treatment, IONP need to reach the tumor in a sufficiently large quantity, using: i) passive targeting, *i.e.* the extravasation of IONP through the blood vessel irrigating the tumor, ii) molecular targeting achieved by a ligand bound to IONP specifically recognizing a cell receptor, and iii) magnetic targeting in which a magnetic field gradient guides IONP towards the tumor. As a whole, targeting efficacy is relatively similar for different targeting, yielding a percentage of injected IONP in the tumor of 5.10^{-4} to 3%, 0.1 to 7%, and 5.10^{-3} to 2.6% for passive, molecular, and magnetic targeting, respectively. For the treatment of iron anemia disease, IONP are captured by the RES, and dissolved into free iron, which is then made available for the organism. For the treatment of cancer, IONP either deliver chemotherapeutic drugs to tumors, produce localized heat under the application of an alternating magnetic field or a laser, or activate in a controlled manner a sono-sensitizer following ultrasound treatment.

KEYWORDS: iron oxide nanoparticle, toxicity, pharmacokinetic, biodistribution, liver toxicity, kidney toxicity, iron anemia.

ABBREVIATIONS:

Admin. Route: Route of administration.

BBB: Selective semi-permeable membrane barrier that separates the circulating blood from the brain and extracellular fluid in the central nervous system.

CKD: Chronic kidney disease.

CE marked: CE marked medical devices, such as those containing nanoparticles, are allowed for commercialization in Europe.

CT: circulation time, i.e. the time required for IONP to flow between two given points;.

$t_{1/2}$: blood half-life, *i.e.* the time it takes for IONP to have their concentration decreased by a factor of 2 following their administration.

CTX: Cyclophosphamide.

DMSA: Dimercaptosuccinic acid

EMA: European Medicines Agency.

EPR: Enhanced permeability and retention effect is a mechanism enabling IONP to accumulate in tumor tissue more than in normal tissues.

FDA: Food and drug agency in USA.

IONP: Iron oxide nanoparticles, composed of a maghemite or magnetite core surrounded by a coating material, displaying superparamagnetic or ferrimagnetic magnetic behaviors, of sizes 1 to 100 nm.

iv: intravenous.

MT: Magnetic targeting or application of a magnetic field gradient on IONP to target the tumor with IONP.

MDT: Molecular drug targeting used to target a tumor.

MTO: Mitoxantrone.

MTX: Methotrexate.

MRI: Magnetic resonance imaging.

MW: Molecular weight.

PVA: Polyvinyl alcohol.

%ID: Percentage of the injected dose that ends up in the tumor.

Quantity admin.: Quantity administered.

RES: Reticuloendothelial system is a network of cells and tissues, in blood, general connective tissue, spleen, liver, lungs, bone marrow, and lymph nodes.

SPIO: Superparamagnetic iron oxide nanoparticles having a thermally unstable magnetic moment.

TA: Targeting agent used to target a tumor.

INTRODUCTION

In the medical field, IONP (iron oxide nanoparticles) have attracted much attention due to several of their appealing properties such as: i) their faculty to efficiently release free iron in the organism and fight against iron anemia disease, (Auerbach2017), ii) the coupling of their magnetic moment with an external magnetic field that improves the quality of the contrast in magnetic resonance imaging (MRI), (DiMarco2007), can yield efficient magnetic drug targeting (MDT), (Janko2013), or produce localized heat in magnetic hyperthermia, (Perigo2015), iii) the absorption of laser light resulting in efficient photothermal therapy, (Estelrich2018), iv) the binding of targeting agents, chemotherapeutic drugs, or sonosentitzers, which can increase the quantity of IONP reaching the tumor and/or enhance anti-tumor activity, (Gobbo2015). Figure 1 summarizes these various medical applications of IONP. Although belonging to a specific category of nano-product, IONP are characterized by a series of different physico-chemical properties: i) amorphous or crystallized structures, (Phu2011), ii), multiple iron oxide compositions and crystallographic structures, such as magnetite (Fe_3O_4) or maghemite (Fe_2O_3), (Salazar2011), iii), different sizes, size distributions, and hydrodynamic diameter, typically comprised between 1 and 100-500 nm, (Wu2008), iv), various shapes or geometries including isotropic ones such as cubic and spherical, (Zhen2011), and elongated ones such as elliptical, (Freitas2015), v), various surface charges, typically comprised between -40 and 30 mV, (Sakukhua2015), vi), magnetic properties most commonly leading to superparamagnetism or ferrimagnetism with unstable or stable magnetic moment, respectively, (Wu2015), vi), the presence of various coating materials, targeting agents, sonosensitizers, and/or chemotherapeutic drugs surrounding the iron oxide core, (Laurent2008). In general, it is possible to tune these properties to adjust IONP biodistribution and activity in the organism, making these nanoparticles an excellent system to foresee efficient treatments of cancer and iron anemia disease. Here, various IONP fabrication methods as well as the main properties of commercialized or CE marked IONP preparations are first described. Second, IONP biodistribution properties as well as the main parameters influencing them are presented. Third, the different types of targeting strategies that enable IONP to reach the tumor in sufficiently large quantity to trigger anti-

tumor activity are highlighted. They include passive targeting through the EPR (Enhanced permeability and retention) effect as well as molecular and magnetic active targeting. Fourth, the mechanisms of actions are explained. They involve the capture of IONP by the RES (reticuloendothelial system) followed by the dissolution of IONP into free iron for the treatment of iron anemia disease. In cancer treatment, they are due to the delivery of anti-cancer drug in the tumor, localized tumor heating under the application of an external alternating magnetic field or laser, or controlled drug release in the tumor following ultrasound exposure.

GENERAL FABRICATION METHODS AND PROPERTIES OF IRON OXIDE NANOPARTICLES

To synthesize IONP, various chemical synthesis have been suggested, which involve: i) co-precipitation by mixing ferrous and ferric salts in an aqueous medium, (Martínez-Mera2007), ii), electrochemistry where an electric current is applied between an anode and a cathode introduced in an electrolyte, the anode oxidizes metal ions of the electrolyte that are further reduced to metal by the cathode with the help of stabilizers, (Khan2000, Ramimoghadam2014), iii), flow injection syntheses by mixing reagents under laminar flow regime in a capillary reactor, (Salazar2006), iv), hydrothermal reactions in which mixed metal hydroxides can be autoclaved to produce nanoparticle powders, (Wan2005), v), laser pyrolysis where a laser heats a mixture of iron precursors and a flowing mixture of gas, (21 Verdaguer1998), vi), high temperature reaction of polyol with an iron source, (Cai2007), vii), sol-gel methods in which precursors undergo hydroxylation and condensation to yield nanometric particles (sol), followed by condensation and polymerization to produce a three-dimensional metal oxide network (wet gel), ending by a heating process that results in a crystallized structure, (Albornoz2006), viii), sonolysis or thermolysis involving the decomposition or collapse of organometallic precursors such as ferrous salts, (Osuna1996), ix), spray pyrolysis in which solutions of ferric salts and a reducing agent in organic solvent is sprayed in reactors leading to the condensation of the aerosol solute and solvent evaporation, (Pecharroman1994).

Whereas IONP are predominantly composed of iron oxide, another material, which is often designated as coating material, either surrounds the iron oxide core of IONP or is mixed with the iron oxide. Such material is used to maintain IONP stability and enable its safe administration. A large number of different coating materials have been added at the same time or following the fabrication of IONP core, such as polysaccharides (Dias2011), acids (Laurent2008, Sahoo2005, boyer2010), polymers (Boyer2010, Laurent2008, karimi2013), dendrimers (Walter2014, Parat2015), carbohydrate (Mahmoudi2011), inorganic (Cui2014, Giakisikli2013) or organic materials (Gautier2013), metals (Giakisikli2013), phosphates (Groult2014), silica (Mahmoudi2011, Alwi2012, Sun2005), dextran (Osborne 2011, Hola2015, Berry2004), or PEG (Gupta2005, Hola2015). Furthermore, the coating material usually contain a functional group, which is able to bind to the surface of IONP core, such as OH (Hola2015, Boyer2010), NH_2 (Hola2015), COOH (Hola2015), thiol (Fauconnier1997), phosphonate (Basly2010), or phosphate (Groult2014). Functions such as OH, NH_2, COOH, and thiol, usually give rise to electrostatic interactions with the iron oxide, whereas phosphates yield covalent binding with the iron oxide.

It goes beyond the scope of this article to describe in all details the various IONP physico-chemical properties, such as IONP composition, size, charges, coating thickness, surface, interaction, geometry, organization, distribution properties. The reader is redirected towards other excellent reviews on these aspects, (Gupta2005, Laurent2008).

COMMERCIALIZED OR CE MARKED FORMULATIONS CONTAINING IRON OXIDE NANOPARTICLES FOR THE TREATMENT OF IRON ANEMIA DISEASE OR CANCER TREATMENT:

For patients suffering from iron anemia disease (IAD) for which orally administered iron does not lead to sufficient efficacy, intravenous administration of the following IONP formulations have been recommended and commercialized (Auerbach2017), (table 1):

- **Dexferrum** (also designated as iron dextran injection), consisting of high molecular weight iron dextran complex at a concentration of 50 mg/mL mixed in solution with sodium chloride for tonicity, (Dexferrum monograph),
- **Feraheme** (also designated as Ferumoxytol or Rienso), consisting of non-stoichiometric magnetite superparamagnetic iron oxide nanoparticles (SPIO) of 16-31 nm and 750 kDa coated with polyglucose sorbitol carboxymethylether, having a chemical formula $Fe_{5874}O_{8752}$-$C_{11719}H_{18682}O_{9933}Na_{414}$, suspended in solution in the presence of mannitol at a pH of 6 to 8, an osmolality of 270-330 mOsm/kg, and a concentration of 30 mg/mL, (Feraheme monograph),
- **Ferrisat** (also designated as Cosmofer, InFeD, iron dextran), made of a slightly viscous sterile liquid complex of ferric hydroxide, dextran, and 0.9% sodium chloride, of pH 5.2-6.5, and concentration of 50 mg/mL, (Infed monograph),
- **Ferrlecit** (sodium ferric gluconate complex in sucrose injection), made of a sodium salt of a ferric iron gluconate complex in alkaline aqueous solution with approximately 20% sucrose w/v (195 mg/mL) and 0.9% w/v benzyl alcohol as preservative, of molecular formula $[NaFe_2O_3(C_6H_{11}O_7)(C_{12}H_{22}O_{11})_5]$, MW 289-440 KDa, mixed in water at a pH of 7.7-9.7, concentration of 12.5 mg/mL, administered at a minimum cumulative dose of 1 gram of elemental iron administered over several sessions, (Ferrlecit monograph).
- **Monofer** (also designated as iron isomaltose), made of iron(III) atoms chelated with carbohydrate, mixed in solution of pH of 5-7 with 0.9% sodium chloride, having a structure resembling that of ferritin, designed to prevent the toxicity of unbound inorganic iron(III), and administered at a dose, which is: i), lower than 1 g for fast administration, *i.e.* within more than 15 minutes or, ii) larger than 1 g for a slow administration, *i.e.* within more than 30 minutes, (Monofer monograph),
- **Venofer®** (iron sucrose injection), made of a complex of polynuclear iron (III)-hydroxide in 30% w/v sucrose without any preservative, of MW ~ 34–60 kDa, proposed structural formula $[Na_2Fe_5O_8(OH)\cdot 3(H_2O)]_n\cdot m(C_{12}H_{22}O_{11})$, where n is the degree of iron polymerization and m is the

number of sucrose molecules associated with the iron (III)-hydroxide, of iron concentration 20 mg/mL, pH ~ 10.5, and osmolarity for injection ~ 1.250 mOsmol/L, (Venofer monograph),

- **Nanotherm®** is a CE marked IONP formulation, consisting of amino-silane coated SPIO of diameter 15 nm, dispersed in water at an iron concentration of 112 mg/mL. It is designed to be administered directly inside brain GBM tumor at a quantity of 200-600 mg of IONP and heated to 42-59 °C by applying an alternating magnetic field of frequency 100 kHz and strength 2.5–18 kA/m, (Maier-Hoff2007, Maier-Hoff2011).

PARAMETERS INFLUENCING THE BIODISTRIBUTION OF IRON OXIDE NANOPARTICLES

The different parameters that influence IONP biodistribution properties in the organism, which are summarized in Figure 2, are the followings:

- **IONP size.** It first has an impact on IONP blood half-life ($t_{1/2}$). Indeed, it was shown that $t_{1/2}$ decreases from $t_{1/2}$ ~ 50 min at 20 nm down to $t_{1/2}$ ~ 20 min at 85 nm. (Kooi2003, Beaumont2009). Second, it influences IONP route of elimination. IONP larger than 200 nm were reported to be degraded by macrophages located in the marginal red pulp zone of the spleen that phagocyte IONP. IONP with sizes lying between 200 nm and 10-15 nm can avoid renal clearance, diffuse through liver or spleen fenestrated sinusoids and be trapped in these organs through macrophage phagocytosis (Feng2018). IONP degradation in the liver is essentially carried out by Kupffer cells or hepatocytes, (Arami2015). IONP captured in the liver are usually internalized by pinocytosis and degraded there, (Huang2010). IONP smaller than 10-15 nm were reported to be captured and degraded by the kidney. The kidney fenestrae act as filters that only allow IONP smaller than ~ 10–15 nm to leave the bloodstream and get rapidly excreted from the body. Third, when IONP are used to treat an individual with a tumor, their size determines their ability to enter (or not) the tumor through the enhanced permeability and retention (EPR) effect. Small IONP can more efficiently than larger ones extravasate from the tumor blood vessels by the EPR effect and diffuse in the tumor. The EPR effect is reported to occur for IONP with a

size lower than ~ 200-300 nm above which NP size becomes significantly larger than the size of the blood vessel holes that irrigate the tumor, (Wang2017).

- **IONP hydrophobicity/hydrophilicity.** Hydrophobic IONP have a shorter circulation time (CT) than hydrophilic ones since plasma proteins can more easily adsorb at their surface, yielding their recognition by the reticuloendothelial system (RES), and removal from blood circulation, (Tong2010). The core of IONP can be coated with hydrophilic molecules such as PEG to reduce opsonization and increase IONP CT.
- **IONP surface charge**. It determines the efficacy of: i), adsorption of plasma proteins at IONP surface leading to IONP recognition and capture by these cells, (Sakulkhu2014), ii), binding of IONP to non-targeted cells yielding nonspecific IONP internalization, (Bachmann2002). Since both of these mechanisms are enhanced for positively charged IONP, these IONP should yield a faster clearance compared with negatively or neutrally charged IONP, although, to the author knowledge, this has not been firmly demonstrated experimentally.
- **IONP core composition (maghemite versus magnetite).** Since degree of oxidation is relatively similar between maghemite and magnetite, it is uncertain that it has a real impact on IONP biodistribution profile.
- **IONP coating.** IONP are coated to enhance their stability, enable their administration, prevent IONP capture by the immune system, or target specific organs. The strength of the interactions between coating and core of IONP determines for how long IONP coating remains associated with the IONP core *in vivo*, *i.e.* coating adsorption yields more rapid coating detachment than covalent binding of the coating, (Arami2015). A general relation between IONP half-life values ($t_{1/2}$) and coating type can't easily be deduced from experimental data due to the large variation of $t_{1/2}$ values reported for the same coating material, *i.e.* 6 min to 21-30 h for dextran, 7 to 8 h for chitosan, 45 min to 62 h for PEG, 8 to 36 min for citrate, (Arami2015). The distribution in $t_{1/2}$ values may be attributed to different coating thicknesses or types of interaction with IONP core observed for the same coating material. A specific coating (inoleic acid, lactobionic acid, PEG, dextran, CMD) can prevent IONP opsonization and capture

by macrophages, and enable IONP to reach the liver or spleen, (Arami2015). Among the different types of coatings, PEG has been the most widely used because of its stabilizing property via steric hindrance, which prevents interaction with blood and serum proteins.

- **IONP administration route.** IONP injected: i), by inhalation, intrapulmonary, intratracheal, or in intranasal route led to IONP retention in the lung without significant adverse effects (Lewinski2013), ii) intravenously resulted in IONP capture by the RES as well as accumulation and/or excretion through liver, spleen, and/or kidney depending on IONP size, (Arami2015), iii), intradermally yielded IONP accumulation in regional lymph nodes, (Longmire2008), iv), orally led to IONP localization in the gastrointestinal (GIT), where IONP with a specific coating can overcome the acidic environment of GIT, diffuse through the liver without capture by Kupffer cells, and enter the general blood circulation system, (Arami2015), v), intra-peritoneal resulted in IONP distribution in liver, lymph nodes and lung, (Pham2018), vi), subcutaneously facilitated high tumor uptake, (Reddy2005), vii) intratumorally resulted in IONP either rapidly leaving the tumor 3 hours following injection to migrate to the bone (Zadnik2014) or remaining in the tumor more than 29 hours following injection (Kossatz2015).
- **Quantity of IONP administered in the organism.** When the quantity of IONP administered (Q_{IONP}) is increased, the value of $t_{1/2}$ globally increases and IONP reach the liver at a later stage. Indeed, as Q_{IONP} increased from 0.0145-0.224 mg/kg to 11-15 mg/kg, $t_{1/2}$ was reported to globally increase from 1-81 to 13-37200 minutes. Furthermore, while for Q_{IONP} ~ 15 µmol Fe.kg^{-1}, IONP reached the liver 1-4 h following IONP injection, they accumulated in this organ at a later stage for Q_{IONP} ~ 150 µmol Fe.kg^{-1}, *i.e.* 8-24 h following IONP administration (Arami 2015).
- **IONP geometry.** Indeed, it was reported that nanoparticles with a large length to width aspect ratio, (Geng2007), possess a longer blood circulation time than their spherical counterparts, (Petros2010). IONP geometry could also possibly determine the organ in which nanoparticles diffuse, with elongated and spherical nanoparticles accumulating predominantly in lymph nodes, (Park2008), and liver, (Zhao2013), respectively.

- **IONP opsonization.** It is another important factor determining the toxicity/biodistribution of these nanoparticles. Opsonization mechanism, which was reported to occur both at IONP core and coating surfaces, seems to depend on: i), protein molecular weight and IONP size with heavier proteins seemingly adsorbing onto larger IONP, (Sakulkhu2014), ii), charges with proteins adsorbing onto IONP surface of opposite charge as that of proteins. For IONP coated with dextran, cationic plasma proteins such as histidine-proline rich glycoprotein (HPRG) and high molecular weight kininogen (HMWK) were observed to bind to anionic magnetite cores, (Simberg2009), while immunoglobulins (IgG) and mannanbinding lectins (MBL) were observed to interact with the cationic dextran coating, (Simberg2009). In general, opsonized IONP were shown to yield longer $t_{1/2}$, CT, and/or clearance values, (Arami2015).

IONP BIODISTRIBUTION AND PHARMACOKINETICS

IONP biodistribution properties depend on the physiological barriers that they encounter, their faculty to cross (or not) these barriers as well as the chosen administration route (see previous section). Biodistribution properties are summarized in table 2 for IONP administered by intravenous, intra-gastric, or intraperitoneal route, to mice, rats, and pig, at a dose comprised between 0.5 to 2000 mg/Kg. When IONP are injected intravenously, they can be captured by white blood cells such as monocytes and residential tissue macrophages, and accumulate in liver and spleen, (Feng2018). Redistribution in these organs depends on the following parameters: i), the time following administration, *i.e.* it was observed to increase during 5-15 hours following IONP injection and then decrease afterwards (Azadkbakht2017), ii), the size of IONP, the smallest (10 nm) and largest (40 nm) IONP were reported to accumulate predominantly in the liver and spleen, respectively (Yang2015), iiii), the quantity of IONP administered with IONP possibly distributing in spleen after saturation of the liver, (Remya2016). In the liver, IONP are phagocytized by Kupffer cells, which degrade and metabolize them partly or fully in dissolved iron and/or in a protein-iron complex, called ferritin, possibly with the help of liver hepatocytes (Gu2012, Briley-Saebo2004). When Kupffer cells are saturated by a too large quantity of IONP, (Arami2015), IONP could be degraded by spleen macrophages. IONP can be found in smaller

quantity than in spleen and liver in other organs such as lung, kidney, heart, bladder, muscle, ovary, colon, muscle, pancreas, intestine, stomach, and uterus, (table 2). When IONP enter an organ, they ultimately may diffuse to the lymph nodes surrounding it, (Thorek2006). Under specific conditions in terms of IONP size, coating, and presence of a specific targeting compound, IONP have been reported to cross several physiological barriers such as the blood brain, (Huang2016), placental (Muller2018), or skin barrier (Musazzi2017). Furthermore, IONP can also target tumors following intravenous administration, either through passive targeting also called enhanced permeability retention (EPR) effect, (Maeda2010), or active targeting using a compound attached to IONP such as peptides (*e.g.* chlorotoxin, RGD, CREKA, bombesin, F_3, A_{54}, LHRH), antibodies (*e.g.* Anti-HER_2, Anti-EGFR/EGFRvIII), and small molecules (*e.g.* folate) that can specifically recognize tumor cells, (Cole2011). Concerning IONP excretion mechanism, although it was suggest that the largest IONP end up in liver, spleen and then feces while the smallest ones are eliminated through kidney and urines, multiple IONP transformations in the organism can possibly yield a different behavior.

TARGETING MECHANISMES OF IRON OXIDE NANOPARTICLE

Passive targeting (EPR effect):

The efficacy of passive targeting, measured by estimating the percentage of injected IONP in tumors resulting from passive targeting of various types of IONP (different charges, coatings, encapsulations, compositions), following intravenous injection of 0.1-4 mg of IONP to mice suffering from different types of tumors, is summarized in table 3. The EPR effect is a consequence of angiogenesis, which leads to highly proliferating endothelial cells with a low density, and to openings of 100-800 nm between these cells. Nanoparticles, which are smaller than 100-800 nm can extravasate or diffuse from the blood vessels into the tumor interstitium. On the one hand, the largest nanoparticle size for which the EPR effect occurs seems to be ~ 200 nm, since nanoparticles larger than 200 nm could be captured by the spleen or liver and not able to reach the tumor. On the other hand, nanoparticles smaller than 30 nm could diffuse back from the tumor to the blood vessel, and be eliminated by the MPS or kidneys, (Sun2014). The range of nanoparticle sizes that yields the most efficient tumor retention is therefore

comprised between 30 and 200 nm. Other nanoparticle parameters can have an impact on EPR efficacy such as : i), the shape of the nanoparticles with spherical nanoparticles apparently diffusing less efficiently through the vascular wall than rod- and bar-shaped nanoparticles, ii) the sleath capacity of the nanoparticles, provided for example by the presence of PEG molecules at nanoparticle surface, leading to prolonged circulation half-life, less protein adsorption, reduction in clearance by the MPS, and thus improved tumor accumulation, iii) the charge of nanoparticle with slightly negatively charged nanoparticles escaping from macrophage endocytosis, and therefore more efficient accumulating in tumor, (Sun2014). To be more efficient, passive targeting needs to overcome the following limitations: i), the in-homogeneous distribution of blood vessels resulting from angiogenesis that yields non-uniform permeability within the whole tumor, ii), its limited efficacy on small tumors or metastases that display reduced angiogenesis, iii), its efficacy of tumor targeting leading to 0.0005-3 % of injected IONP in tumor (table 3) and to 20-30% more nanoparticles in tumors compared with other organs, (Kobayashi2014). While the EPR effect was reported to lack efficacy in some studies, (Wilhelm2016), it was described as enabling nanoparticles to achieve much improved targeting efficacy compared with other drugs in some other studies, (Golombek2018).

Molecular targeting:

Active targeting usually occurs after nanoparticles have diffused to the tumor by passive targeting, making the efficacy of active targeting dependent on that of the EPR effect. The principle of active targeting relies on interactions between a ligand attached to the nanoparticles and a receptor located at cell surface. Examples of ligands are: i) various monoclonal antibodies, *e.g.* 610, L6, HER/Neu, A7, and antibody to prostate specific membrane antigen, ii) transferrin, iii) various peptides , *e.g.* EPPT, Chlorotoxin, F3, and CREKA, iv) folic acid and methotrexate, v) Herceptin, vi) RGD, vii) luteinizing hormone releasing hormone (LHRM), which target: i) antigens of different tumor cells, ii) transferrin receptor, iii) Underglycosylated mucin-1 antigen (uMUC-1), membrane-bound matrixmetalloproteinase-2 (MMP-2), Surface-localized tumor vasculature, Clotted plasma proteins, iv) folate receptor, v) Her-2/neu receptors, vi) $\alpha_v ß_3$ integrins, and vii) LHRH receptor, respectively,

(Peng2008). To be efficient, active targeting seems to require the combination of a rather larger number of properties such as: a larger quantity of receptors on cancer than non-cancer cells, the availability of receptors on cancer cell surface, the successful binding of ligands to receptors followed by internalization of the complex ligand-IONP in cancer cells, an homogenous distribution of receptors within the tumor, the availability of cancer cells used for *in vitro* assessment of ligand/receptor interactions displaying similar properties than cancer cells found in a patient's tumor, a sufficiently large fraction of tumor cells expressing a receptor specific to the used ligand. Table 4 summarizes the efficacy of active targeting reached by administering intravenously to mice suspensions containing between 0.073 and 0.5 mg of IONP combined with different types of targeting agents (TA), *i.e.* various antibodies (PSMA antibody, anti-GD2 antibody, Trastuzufab, antibody fragment Ffab), biotin, folate, and RGD. It was reported that the administration of IONP with TA increases the percentage of IONP in tumor, *e.g.* the percentage of injected IONP increases from 1.4% without Trastuzufab to 3% with Trastuzufab, (Dong2015). Interestingly, such improvement was observed for IONP of the lowest size (30 nm), and not for those of 100 nm, suggesting that as for the EPR effect, the efficacy of active targeting may depend on nanoparticle size, (Dong2015). Another interesting study has shown that by adding carboxy-methyl-dextran (CMD) at the surface of the nanoparticles, which increases IONP circulation time, the efficacy of active targeting of IONP toward KB tumors increases from 4% using IONP associated with Ffab to 7% using IONP combined with Ffab and CMD. Due to the large number of parameters that needs to be under control to make active targeting efficient, it is unsurprising that various studies report very different efficacy for active targeting (table 4). As a whole, it however appears that active targeting is promising and therefore deserves to be tested on humans.

Magnetic targeting:

The principle of magnetic targeting relies on the application of a magnetic field gradient that results in a magnetic force, F, which is sufficiently strong to drive IONP towards the tumor, usually in an opposite direction from that of the blood flow. Using a simplified approach that does not take into consideration the complexity of biological systems but gives an idea of the parameters onto which the magnetic force

358 depends, it was suggested that: $F = M_S.V.\nabla B$, where M_S and V are the saturating magnetization and
359 volume of IONP, respectively, and ∇B is the magnetic field gradient applied on IONP,
360 (Bietenbeck2016). According to this relation, the magnetic force is the strongest when the saturating
361 magnetization, volume of nanoparticles, and ∇B reach the largest values. In fact, although the values of
362 these three parameters should be large enough for magnetic targeting to be efficient, they can't exceed
363 certain values, *e.g.* first the volume of IONP should remain below the volume at which IONP switch
364 from a single to a multi domain magnetic behavior, second the saturating magnetization may be
365 increased by doping iron oxide nanoparticles with various materials such as cobalt but these materials
366 are usually toxic and can't easily be used for medical application, third too large magnetic gradients
367 should be avoided since they could also possibly prevent efficient targeting. The efficacy of magnetic
368 targeting further depends on other parameters such as blood flow or viscosity, and SPION concentration
369 in the blood. Regarding the properties of the magnetic field required to reach efficient magnetic
370 targeting, most studies report the use an external and static magnetic field to guide IONP toward the
371 tumor region, whose strength is between 0.2 and 0.6 T. The value of the magnetic field gradient, which
372 is more directly linked to the efficacy of magnetic targeting than that of the magnetic field strength, is
373 usually not given. One study mentions the use of a magnetic field gradient of 100 T/m to drive IONP
374 through arteries, (Bietenbeck2016). Interestingly, efficient magnetic targeting was observed for different
375 durations of application of the magnetic field, which was typically comprised between 30 min,
376 (Aguiar2017) and 48 h (Estelrich2015). Practically, for efficient magnetic targeting, different types of
377 magnets such as neodymium magnet or electromagnet, (Aguiar2017), can be attached at the surface of
378 the skin, located above the tumor of the treated animals. Table 5 summarizes the efficacy of magnetic
379 targeting of various types of IONP (different coatings, charges, compositions) injected intravenously or
380 intra-arterially to mice or rats at a dose comprised between 0.3 mg and 4 mg per animal, under the
381 application of a magnetic field usually orientated in the direction of the tumor of strength comprised
382 between 0.32 T and 1.2 T. It was shown in several studies that magnetic targeting improves the efficacy
383 of targeting, *i.e.* the percentage of injected IONP ending up in the tumor increases from 5.10^{-3} to 5.10^{-}

384 [2]% for G100 starch coated IONP targeting 9L glioma tumor, from 2 to 6% for IONP encapsulated in
385 nanocapsule targeting CT-26 colon tumor, from 0.1 to 0.5-0.8% for IONP coated with amino groups
386 targeting C6 glioma tumors, from 3 to 7% for IONP embedded in nano-bubbles targeting CT26 colon
387 tumors, and from 5 to 12% for IONP of composition ZnMnFeO targeting 4T1 tumor (table 5).
388 Interestingly, it was also reported that several IONP properties can further improve the efficacy of
389 magnetic targeting such as: i) the application of focused ultrasound (FUS) for the targeting of C6 glioma
390 brain tumors that possibly favors the diffusion of IONP to brain tumor by opening the blood brain
391 barrier, resulting in an increase in the percentage of injected IONP in the tumor from 2% using MT
392 without FUS to 6% using MT with FUS, ii) the coating surrounding IONP that can increase the
393 circulation time of IONP or contribute to an active targeting mechanism, resulting in an increase of the
394 percentage of injected IONP in the tumor from 1% using IONP without a specific coating to 3% using
395 IONP coated with β-glucosidase that targets amygdalin and furthermore to 6.5% using IONP coated
396 with both β-glucosidase and PEG (Zhou2014). As a whole, the percentage of injected IONP that ends
397 up in the tumor following magnetic targeting varies quite a lot depending on the tested condition and
398 lies between 5.10^{-3} and 2.6%. Given the values of these percentages, the majority of IONP does not end
399 up in the tumor but in other parts of the organism, and one should therefore verify that despite the small
400 values of these percentages, IONP are located in a sufficiently large quantity in the tumor to be able to
401 trigger anti-tumor activity.

402 **MECHANISME OF ACTION OF IONP IN TREATMENT OF IRON ANEMIA DISEASE**

403 IONP can be used for the treatment of iron anemia disease, possibly associated with chronic kidney
404 disease (CKD), and combined (or not) with other drugs such as erythropoietin. They are usually
405 prescribed when oral administration of iron based drugs is not sufficiently efficient. IONP can be
406 administered using a typical minimum total dose of 1 g of elemental iron. Sequential sessions can be
407 used to increase the quantity of injected IONP. The mechanism of action of these IONP relies on the
408 capture of these nanoparticles by the RES, which is believed to separate iron from other materials
409 comprised in IONP (dextran for dexferrum and ferrisat, polyglucose sorbitol carboxymethylether for

feraheme, gluconate for ferrlecit, carbohydrate for monofer, amono-silane for nanotherm) and then make iron bio-available for the organism. These IONP were reported to mainly distribute in blood, extravascular fluid, liver, spleen and bone marrow. Iron could be trapped and possibly slowly released in the bone marrow, liver, and/or spleen, and then get bound to or form hemosiderin, ferritin, or transferrin, which can store or transport iron in the organism. This treatment was also described as increasing the hemoglobin concentration in the organism. These IONP are characterized by large $t_{1/2}$ values, *i.e.* $t_{1/2}$ ~ 59 hours for dexferrum, $t_{1/2}$ ~ 15 hours for Feraheme, $t_{1/2}$ ~ 5-20 hours for Ferrisat, $t_{1/2}$ ~ 7-12 hours for Injectafter, $t_{1/2}$ ~ 1-4 days for Monofer, $t_{1/2}$ ~ 6 h for Venofer, (monographs of these various drugs). Iron originating from these IONP usually displays negligible elimination by the kidneys. Other material than iron, such as IONP coating, can be excreted through urines and/or feces or be metabolized. The low toxicity of these IONP was highlighted by large LD_{50} values in mice, *e.g.* above 500 mg/kg (Monogr. Dexferrum).

IONP FOR DELIVERY OF ANTI-CANCER DRUGS IN THE ABSENCE OF AN EXTERNAL SOURCE OF EXCITATION

First, IONP may be used to increase the probability of success of cancer gene therapy. In this case, IONP can be coated with polymers, such as PEI, PEG, or chitosan, or made positively charged to bind IONP with negatively charged nucleic acids, belonging either to DNA plasmids or to siRNA. The use of IONP favors cellular internalization of DNA or siRNA, which further promotes transfection of DNA or diffusion of siRNA in the cytoplasm followed by the inhibition of mRNA translation. In this way, the normal behavior of cells could be restored by delivering DNA plasmids that can replace damaged genes or siRNA that can prevent the expression of oncogenes, (Kievit2011).

Second, another application of IONP is the treatment of cancer by protein therapy. IONP can be associated or linked to proteins to favor the antitumor mechanisms such as: i) the blocking of cell surface receptors by using for example III (EGFRvIII) antibody that inhibit the cellular receptor EGFRvIII, (Hadjipanayis2010), ii) CTX that decreases tumor cell proliferation, (Velseh2009), iii) Cytochrome c that favors tumor cell apoptosis, (Santra2010), iv) interferon gamma (IFNγ) that triggers

an anti-tumor immune activity, (Mejias2008). Compared with the use of free proteins (without IONP), proteins associated with IONP should be less easily metabolized or cleared, be delivered more efficiently to cancer cells, be protected from protease degradation, or more efficiently interact with parts of cancer cells such as cell receptors by being located on IONP surface.

Third, IONP can enhance chemotherapy efficacy. As for gene and protein therapy, the underlying mechanism relies on enhanced interaction between chemotherapeutic drugs and cells by linking these drugs to IONP. By using IONP, chemotherapeutic drugs can have a better access to several parts of the cells such as the cell nucleus to inhibit DNA replication, or mitochondria to prevent mitochondrial activity. As an example, IONP conjugated to the anti-cancer drug MTO was administered intra-arterial into rabbits, leading to drug accumulations in the tumor, complete tumor remissions, and to an apparent cure among 30% of treated animals, (Tietze2013).

IONP and chemotherapeutic drugs can be linked together in different ways, (El-Boubbou2018), *i.e.* through:

- Electrostatic, dipole–dipole, or van der Waals forces interactions between drugs and IONP, resulting in IONP-drug complexes that are relatively simple to fabricate, prevent drug covalent modification, and enable a control of drug delivery in the desired target of the organism,
- Drug encapsulation, *e.g.* by coating IONP core with a porous material such as silica, in which drugs can be inserted, or by making phospholipid bilayers inside which IONP can be inserted, preventing drug degradation, limiting drug side effects, and yielding controlled drug release.
- Covalent binding between IONP and drugs, *e.g.* using amine functionalized IONP that are covalently conjugated to MTX, and enable drug release at an acidic pH of 2, (Kohler2005).

Compared with non-covalent bindings, covalent ones present both advantages and drawbacks. On the one hand, they are very strong and can usually more efficiently resist physiological disturbance and therefore yield a larger life time in the bloodstream. On the other hand, they can be non-biocompatible depending on the chemicals used for the binding, non-cleavable after IONP have reached their target, or enable only a small quantity of drugs attached to each IONP.

IONP TRIGGERING ANTI-CANCER ACTIVITY IN THE PRESENCE OF AN EXTERNAL SOURCE OF EXCITATION

The most widely used energy source to excite IONP has been the alternating magnetic field, in a treatment method called magnetic hyperthermia, (Obaidat2015, Chang2018, Giustini2010, Perigo2015). When IONP are exposed to such magnetic field, it either produces the rapid inversion of the magnetic moment or physical rotation of IONP. Both moderate heating, at typically 41-46 °C, and other non-thermal effects, such as nanoparticles movements, have been reported to result from such excitation and yield anti-tumor activity. Typical values of the magnetic field strength and frequency that need to be applied to produce efficient magnetic hyperthermia are larger than 5-20 mT and 50-100 kHz, respectively. In general, the strength and frequency of the magnetic field should remain below 20 mT and 100 kHz to avoid non-localized heating that can occur outside of the nanoparticle regions, due to Foucault currents produced by AMF of large strength and frequency. IONP have been administered intra-tumorally or intravenously to treat different types of mouse tumors, and produced anti-tumor activity, (Hayashi2013, Huang2013). Clinical trials are ongoing on patients suffering from glioblastoma to evaluate the efficacy of this treatment, (Maier-Hoff2007, Maier-Hoff2010).

The laser is another excitation source that can be applied on IONP to heat the tumor. A laser wavelength of 808 nm, which yields minimal laser absorption by tissues, as well as a laser power density of typically 1-5 W/cm^2, were reported to yield efficient heat production by IONP, (Esterlich2018). As an example of the efficacy of such treatment, when C6 tumors were subcutaneously grown under the skin of mice and injected with 0.2 mg of IONP followed by 5 minutes tumor laser exposure (825 nm, 1.5 W/cm^2), it prevented tumor growth, (Wang2018).

In the case of ultrasound tumor treatment, it was also suggested to use IONP combined with a sonosensitizer to trigger anti-tumor activity, (Qian2016). Indeed, when SkBr3 breast tumors of 100 mm^3 were injected intravenously with 0.4 mg of IONP conjugated with PEG and Rose Bengal sonosensitizer followed first by the application of a magnetic field on IONP to enhance tumor targeting and then by tumor ultrasound irradiation at 2 W during 60 seconds 24 h post injection, it led to an increase of the

tumor temperature from 31 °C to 48 °C and to a decrease of tumor size within one month following treatment (Chen2016).

CONCLUSION

In this review, the different methods of IONP fabrication as well as the various IONP physico-chemical properties are briefly presented. IONP are currently commercialized or CE marked for treatments of iron anemia or cancer diseases. For these applications, they can be administered to patients, at doses that can exceed 1 gram per patient in some specific conditions.

The different parameters that influence iron oxide nanoparticle toxicity and biodistribution are:

- **IONP size.** It that has an impact on: i) $t_{1/2}$ values, *i.e.* $t_{1/2}$ increases with decreasing IONP sizes, ii), the route of elimination, *i.e.* IONP > 200 nm are degraded in spleen, 10 nm < IONP < 200 nm are eliminated in liver and spleen, while IONP < 10 nm are excreted through kidney.
- **IONP Hydrophobic/Hydrophilic properties.** Hydrophobic IONP yields a shorter circulation time than hydrophilic ones.
- **IONP surface charge.** Positively charged IONP have a faster clearance than negatively or neutrally charged ones.
- **IONP coating.** IONP specific coating, such as PEG, can prevent nanoparticle capture by macrophages.
- **IONP administration route.** It determines in which organ IONP distribute and how they are eliminated.
- **Opsonization.** When IONP are opsonized or when their quantity administered increases, it can lead to an increase in $t_{1/2}$ values.

Concerning the use of IONP for the treatment of iron anemia, it necessitates a sufficiently large IONP circulation time to enables efficient IONP capture by the RES followed by IONP dissolution into free iron. This can be achieved by choosing appropriate IONP properties, in particular IONP coating and IONP size. With regard to cancer treatment with IONP, it necessitates that a sufficiently large quantity

of IONP reaches the tumor. For that, different types of targeting strategies have been tested. Although molecular and magnetic targeting do not seem to improve in all cases targeting efficacy compared with passive targeting, it seems that the quantity of IONP in the tumor is sufficient to trigger anti-tumor activity using IONP for the delivery of chemotherapeutic drugs in the tumor, localized heat in the tumor following the application of an alternating magnetic field or laser, or the activation of a sonosensitizer under ultrasound exposure.

ACKNOWLEDGMENT: We would like to thank the BPI (*''banque publique d'investissement, France''*), the region of Paris (*''Paris Région Entreprise, France''*), the French Research Tax Credit program (*''crédit d'impôt recherche''*), the incubator Paris Biotech Santé, the ANRT (CIFRE 2014/0359, CIFRE 2016/0747, CIFRE 2013/0364, CIFRE 2015/976), the Eurostars programs (Nanoneck-2 E9309 and Nanoglioma E11778), the AIR program (*''aide à l'innovation responsable''*) from the region of Paris (A1401025Q), the ANR (*''Agence Nationale de la Recherche''*) Méfisto, as well as the Universities Paris 6 and Paris 11. We also would like to thank the Nomis Foundation and Markus Reinhard for their support.

REFERENCES:

Abdollah MRA, Carter TJ, Jones C, Kalber TL Rajkumar V, Tolner B, Gruettner C, Zaw-Thin, Baguña Torres J, Ellis M, Robson M, Pedley RB, Mulholland P, de Rosales RTM, Chester KA. Fucoidan Prolongs the Circulation Time of Dextran-Coated Iron Oxide Nanoparticles. *ACS Nano* 2018, 12: 1156−1169.

Aguiar MFDP, Mamani JB, Felix TK, Dos Reis RF, Da Silva HR, Nucci LP, Nucci-da-Silva MP, Gamarra F. Magnetic targeting with superparamagnetic iron oxide nanoparticles for *in vivo* glioma. *Nanotechnol Rev* 2017, 6: 449–472.

Albornoz C, Jacobo SE. Preparation of a biocompatible magnetic film from an aqueous ferrofluid. *J. Magn. Magn. Mat.* 2006, 305: 12-15.

Al-Jamal KT, Bai J, Wang JTW, Protti A, Southern P, Bogart L, Heidari H, Li X, Cakebread A, Asker D, Al-Jamal WT, Shah A, Bals S. Magnetic Drug Targeting: Preclinical in Vivo Studies, Mathematical Modeling, and Extrapolation to Humans. *Nano Lett.* 2016, 16: 5652−5660.

Alwi R, Telenkov S, Mandelis A, Leshuk T, Gu F, Oladepo S, Michaelian K. Silica-coated super paramagnetic iron oxide nanoparticles (SPION) as biocompatible contrast agent in biomedical photoacoustics. *Biomedical Optics Express.* 2012, 3: 2500-2509.

Arami H, Khandhar A, Liggitt D, Krishnan KM. In vivo delivery, pharmacokinetics, biodistribution and toxicity of iron oxide nanoparticles. *Chem. Soc. Rev.* 2015, 44: 8576-8607.

Auerbach M, Macdougall I. The available intravenous iron formulations: History, efficacy, and toxicology. *Hemadialysis International* 2017, 21: S83-S92.

Azad BB, Banerjee SR, Pullambhatla M, Lacerda S, Foss CA, Wang Y, Ivkov R, Pomper MG. Evaluation of a PSMA-targeted BNF nanoparticle construct. *Nanoscale* 2015, 7: 4432–4442.

Azadkbakht B, Afarideh H, Ghannadi-Maragheh M, Bahrami-Samani A, Yousefnia H. Absorbed doses in humans from 188Re-Rituximab in the free form and bound to superparamagnetic iron oxide nanoparticles: Biodistribution study in mice. *Applied Radiation and Isotopes*. 2018, 131: 96–102.

553 Bachmann R, Conrad R, Kreft B, Luzar O, Block W, Flacke S, Pauleit D, Traber F, Gieseke J, Saebo K,
554 Schild H. Evaluation of a New Ultrasmall Superparamagnetic Iron Oxide Contrast Agent Clariscan,
555 (NC100150) for MRI of Renal Perfusion: Experimental Study in an Animal Model. *Journal of magnetic*
556 *resonance imaging* 2002, 16:190–195.
557 Baiu DC, Artz NS, McElreath MR, Menapace BD, Hernando D, Reeder SB, Grüttner C, Otto M. High
558 specificity targeting and detection of human neuroblastoma using multifunctional anti-GD2 iron-oxide
559 Nanoparticles. *Nanomedicine* 2015, 10: 2973–2988.
560 Basly B, Felder-Flesch D, Perriat P, Billotey C, Taleb J, Pourroy G, Begin-Colin S. Dendronized iron
561 oxide nanoparticles as contrast agents for MRI. *Chem. Commun.* 2010, 46: 985-987.
562 Beaumont M, Lemasson B, Farion R, Segebarth C, Rémy C, Barbier EL. Characterization of tumor
563 angiogenesis in rat brain using iron-based vessel size index MRI in combination with gadolinium-based
564 dynamic contrast-enhanced MRI. *Journal of Cerebral Blood Flow & Metabolism* 2009, 29: 1714–1726.
565 Beckmann N, Cannet C, Babin AL, Blé FX, Zurbruegg S, Kneuer R, Dousset V. In vivo visualization of
566 macrophage infiltration and activity in inflammation using magnetic resonance imaging. *WIREs*
567 *Nanomedicine and Nanobiotechnology* 2009, 1: 272-298.
568 Berry CC, Wells S, Charles S, Aitchison G, Curtis ASG. Cell response to dextran-derivatised iron oxide
569 nanoparticles post internalization. *Biomaterials* 2004, 25: 5405–5413.
570 Bietenbeck, M, Florian A, Faber C, Sechtem U, Yilmaz A. Remote magnetic targeting of iron oxide
571 nanoparticles for cardiovascular diagnosis and therapeutic drug delivery: where are we now?
572 *International Journal of Nanomedicine* 2016, 11: 3191–3203.
573 Boyer C, Whittaker MR, Bulmus V, Liu J, Davis TP. The design and utility of polymer-stabilized iron-
574 oxide nanoparticles for nanomedicine applications. *NPG Asia Mater.* 2010, 2: 23–30.
575 Briley-Saebo K, Bjornerud A, Grant D, Ahlstrom H, Berg T, Kindberg GM. Hepatic cellular
576 distribution and degradation of iron oxide nanoparticles following single intravenous injection in rats:
577 implications for magnetic resonance imaging. *Cell Tissue Res* 2004, 316: 315–323.

578 Cai W, Wan J. Facile synthesis of superparamagnetic magnetite nanoparticles in liquid polyols. *Journal*
579 *of Colloid and Interface Science* 2007, 305: 366–370.
580 Chang D, Lim M, Goos JACM, Qiao R, Ng YY, Mansfeld FM, Jackson M, Davis TP, Kavallaris M.
581 Biologically Targeted Magnetic Hyperthermia: Potential and Limitations. *Frontiers in Pharmacology* 9:
582 831.
583 Chen D, Jiang M, Li N, Gu H, Xu Q, Ge J, Xia X, Lu J. Modification of magnetic silica/iron oxide
584 nanocomposites with fluorescent polymethacrylic acid for cancer targeting and drug delivery. *J. Mater.*
585 *Chem.* 2010, 20: 6422–6429.
586 Chen YW, Liu TY, Chang PH, Hsu PH, Liu HL, Lina HC, Chen SY. A theranostic nrGO@MSN-ION
587 nanocarrier developed to enhance the combination effect of sonodynamic therapy and ultrasound
588 hyperthermia for treating tumor. *Nanoscale* 2016, 8: 12648-12657.
589 Chertok B, David AE, Huang Y, Yang VC. Glioma selectivity of magnetically targeted nanoparticles: A
590 role of abnormal tumor hydrodynamics. *Journal of Controlled Release* 2007, 122: 315–323.
591 Chertok B, David AE, Yang VC. Polyethyleneimine-modified iron oxide nanoparticles for brain tumor
592 drug delivery using magnetic targeting and intra-carotid administration. *Biomaterials* 2010, 31: 6317-
593 6324.
594 Cole AJ, David AE, Wang J, Galban CJ, Hill HL, Yang VC. Polyethylene glycol modified, cross-linked
595 starch-coated iron oxide nanoparticles for enhanced magnetic tumor targeting. *Biomaterials* 2011, 32:
596 2183-2193.
597 Cui X, Belo S, Kruger D, Yan Y, Rosales RTM, Jeuregui-Osoro M, Ye H, Su S, Mathe D, Kovacs N,
598 Horvath I, Semjeni M, Sunassee K, Szigeti K, Green MA, Blower PJ. Aluminium hydroxide stabilised
599 $MnFe_2O_4$ and Fe_3O_4 nanoparticles as dual-modality contrasts agent for MRI and PET imaging.
600 *Biomaterials* 2014, 35: 5840-5846.
601 Dan M, Cochran DB, Yokel RA, Dziubla TB. Binding, Transcytosis and Biodistribution of Anti-
602 PECAM-1 Iron Oxide Nanoparticles for Brain-Targeted Delivery. Plos One 2013, 8: e81051.

603 Dias AMGC, Hussain A, Marcos AS, Roque ACA. A biotechnological perspective on the application of
604 iron oxide magnetic colloids modified with polysaccharides. *Biotechnology Advances* 2011, 29: 142–
605 155.
606 DiMarco M, Guilbert I, Port M, Robic C, Couvreur P, Dubernet C. Colloidal stability of ultrasmall
607 superparamagnetic iron oxide (USPIO) particles with different coatings. *International Journal of*
608 *Pharmaceutics* 2007, 331: 197–203.
609 Dong CN, Tate JA, Kett WC, Batra J, Demidenko E, Lewis LD, Hoopes PJ, Gerngross TU, Griswold
610 KE. Tumor Cell Targeting by Iron Oxide Nanoparticles Is Dominated by Different Factors *In Vitro*
611 versus *In Vivo. PLOS one* 2015, DOI:10.1371/journal.pone.0115636.
612 Edge D, Shortt CM, Gobbo OL, Teughels S, Prina-Mello A, Volkov Y, MacEneaney P, Radomski MW,
613 Markos F. Pharmacokinetics and bio-distribution of novel super paramagnetic iron oxide nanoparticles
614 (SPIONs) in the anaesthetized pig. *Clinical and Experimental Pharmacology and Physiology* 2016, 43:
615 319–326.
616 El-Boubbou K. Magnetic iron oxide nanoparticles as drug carriers: preparation, conjugation and
617 delivery. *Nanomedicine* 2018, DOI:10.2217/nnm-2017-0320.
618 El-Kharrag R, Amin A, Hisaindee S, Greish Y, Karam S. Development of a therapeutic model of
619 precancerous liver using crocin-coated magnetite nanoparticles. *International journal of oncology* 2017,
620 50: 212-222.
621 Elmore S. Apoptosis: A Review of Programmed Cell Death. *Toxicol Pathol.* 2007, 35: 495–516.
622 Escamilla-Rivera V, Uribe-Ramirez, Gonzalez-Pozos S, Lozano O, Lucas S, Vizcaya-Ruiz A. Protein
623 corona acts as a protective shield against Fe3O4-PEG inflammation and ROS-induced toxicity in human
624 macrophages. *Toxicology Letters* 2016, 240: 172–184.
625 Estelrich J, Busquets MA. Iron Oxide Nanoparticles in Photothermal Therapy. *Molecules* 2018, 23:
626 1567.

627 Fan C-H, Ting C-Y, Lin HJ, Wang CH, Liu HL, Yen TC, Yeh CK. SPIO-conjugated, doxorubicin-
628 loaded microbubbles for concurrent MRI and focused-ultrasound enhanced brain-tumor drug delivery.
629 *Biomaterials* 2013, 34: 3706-3715.
630 Fan Y, Li C, Li F, Chen D. pH-activated size reduction of large compound nanoparticles for *in vivo*
631 nucleus-targeted drug delivery. *Biomaterials* 2016, 85: 30-39.
632 Fauconnier N, Pons JN, Roger J, Bee A. Thiolation of Maghemite Nanoparticles by Dimercaptosuccinic
633 Acid. *Journal of colloid and interface science* 1997, 194: 427–433.
634 Feng Z, Zhao G, Yu L, Gough D, Howell SB. Preclinical eYcacy studies of a novel nanoparticle-based
635 formulation of paclitaxel that out-performs Abraxane. *Cancer Chemother Pharmacol* 2010, 65:923-930.
636 Feng Q, Liu Y, Huang J, Chen K, Huang J, Xiao K. Uptake, distribution, clearance, and toxicity of iron
637 oxide nanoparticles with different sizes and coatings. Scientific reports 2018, 8:2082.
638 Fernández-Bertólez N, Costa C, Brandao F, Kilic G, Teixeira JP, Pasaro E, Laffon B, Valdiglesias V.
639 Neurotoxicity assessment of oleic acid-coated iron oxide nanoparticles in SH-SY5Y cells. *Toxicology*
640 2018, 406–407:81–912018.
641 Freitas J, Branco RM, Lisboa IGO, Costa TP, Campos MGN, Junior MJ, Marques RFC. Magnetic
642 Nanoparticles Obtained by Homogeneous Coprecipitation Sonochemically Assisted. *Materials*
643 *Research.* 2015, 18: 220-224.
644 Gautier J, Allard-Vannier E, Hervé-Haubert K, Soucé M, Chourpa I. Design strategies of hybrid
645 metallic nanoparticles for theragnostic applications. *Nanotechnology* 2013, 24:432002.
646 Geng Y, Dalhaimer P, Cai S, Tsai R, Tewari M, Minko T, Discher DE. Shape effects of filaments
647 versus spherical particles in flow and drug delivery. *Nat Nanotechnol*. 2007, 2: 249–255.
648 Giakisikli G, Anthemidis AN. Magnetic materials as sorbents for metal/metalloid preconcentration
649 and/or separation. A review. *Analytica Chimica Acta* 2013, 789:1-16.
650 Giustini AJ, Ivkov R, Hoopes PJ. Magnetic nanoparticle biodistribution following intratumoral
651 administration. *Nanotechnology* 2011, 22: 345101.

652 Gobbo OL, Sjaastad K, Radomski MW, Volkov Y, Prina-Mello A. Magnetic Nanoparticles in Cancer
653 Theranostics. *Theranostics* 2015, 5: 1249-1263.
654 Golombek SK, May JN, Theek B, Appold L, Drude N, Kiessling F, Lammers T. Tumor Targeting via
655 EPR: Strategies to Enhance Patient Responses. *Adv. Drug Deliv. Rev.* 2018, 130: 17–38.
656 Groult H, Ruiz-Cabello J, Lechuga-Vieco AV, Mateo J, Benito M, Bilbao I, Martinez-Alcazar MP,
657 Lopez JA, Vasquez J, Herranz FF. Phosphatidylcholine-Coated Iron Oxide Nanomicelles for In Vivo
658 Prolonged Circulation Time with an Antibiofouling Protein Corona. *Chem. Eur. J.* 2014, 20: 16662-
659 16671.
660 Gu L, Fang RH, Sailor MJ, Park J-H. In Vivo Clearance and Toxicity of Monodisperse Iron Oxide
661 Nanocrystals. *ACS Nano.* 2012, 6: 4947-4954.
662 Gupta AK, Gupta M. Synthesis and surface engineering of iron oxide nanoparticles for biomedical
663 applications. *Biomaterials* 2005, 26: 3995-4021.
664 Hadjipanayis CG, Machaidze R, Kaluzova M, Wang L, Schuette AJ, Chen H, Wu X, Mao H. EGFRvIII
665 antibody-conjugated iron oxide nanoparticles for magnetic resonance imaging-guided convection-
666 enhanced delivery and targeted therapy of glioblastoma. *Cancer Res.* 2010, 70: 6303–6312.
667 Hanot CC, Choi YS, Anani TB, Soundarrajan D, David AE. Effects of Iron-Oxide Nanoparticle Surface
668 Chemistry on Uptake Kinetics and Cytotoxicity in CHO-K1 Cells. *Int. J. Mol. Sci.* 2016, 17, 54;
669 doi:10.3390/ijms17010054.
670 Hayashi K, Nakamura M, Sakamoto W, Yogo T, Miki H, Ozaki S, Abe M, Matsumoto T, Ishimura1 K.
671 Superparamagnetic Nanoparticle Clusters for Cancer Theranostics Combining Magnetic Resonance
672 Imaging and Hyperthermia Treatment. *Theranostics* 2013, 3: 366-376.
673 Hola K, Markova Z, Zoppellaro G, Tucek J, Zboril R. Tailored functionalization of iron oxide
674 nanoparticles for MRI, drug delivery, magnetic separation and immobilization of biosubstances.
675 *Biotechnology Advances.* 2015, 33: 1162–1176.
676 Huang G, Diakur J, Xu Z, Wiebe LI. Asialoglycoprotein receptor-targeted superparamagnetic iron oxide
677 Nanoparticles. *International Journal of Pharmaceutics* 2008, 360: 197–203.

678 Huang HS, Hainfeld JF. Intravenous magnetic nanoparticle cancer hyperthermia. *International Journal*
679 *of Nanomedicine* 2013, 8: 2521–2532.
680 Huang B, Zhang H, Gu L, Ye B, Jian Z, Stary C, Xiong X. Advances in Immunotherapy for
681 Glioblastoma Multiforme. *Journal of Immunology Research* 2017, Article ID 3597613.
682 Jain TK, Reddy MK, Morales MA, Leslie-Pelecky DL, Labhasetwar V. Biodistribution, Clearance, and
683 Biocompatibility of Iron Oxide Magnetic Nanoparticles in Rats. *Molecular Pharmaceutics* 2008, 5:
684 316–327.
685 Janko C, Durr S, Munoz LE, Lyer S, Chaurio R, Tietze R, Von Lohneysen S, Shorn C, Herrmann M,
686 Alexiou C. Magnetic Drug Targeting Reduces the Chemotherapeutic Burden on Circulating Leukocytes.
687 *Int. J. Mol. Sci.* 2013, 14: 7341-7355.
688 Jia Z, Song L, Zang F, Song J, Zhang W, Yan C, Xie J, Ma Z, Ma M, Teng G, Gu N, Zhang Y. Active-
689 target T1-weighted MR Imaging of Tiny Hepatic Tumor via RGD Modified Ultra-small Fe3O4
690 Nanoprobes. *Theranostics* 2016, 6: 1780-1791.
691 Karathanasis E, Ghaghada KB. Crossing the barrier: Treatment of brain tumors using nanochain
692 particles. *Wiley Interdiscip Rev Nanomed Nanobiotechnol.* 2016, 8: 678–695.
693 Karimi Z, Karimi L, Shokrollahi H. Nano-magnetic particles used in biomedicine: Core and coating
694 materials. *Materials Science and Engineering C* 2013, 33: 2465–2475.
695 Khan HR, Petrikowski K. Anisotropic structural and magnetic properties of arrays of $Fe_{26}Ni_{74}$
696 nanowires electrodeposited in the pores of anodic alumina. *Journal of Magnetism and Magnetic*
697 *Materials* 2000, 215-216: 526-528.
698 Kievit FM, Zhang M. Surface Engineering of Iron Oxide Nanoparticles for Targeted Cancer Therapy.
699 *Acccounts of chemical research* 2011, 44: 853-862.
700 Kim JE, Shin JY, Cho MH. Magnetic nanoparticles: an update of application for drug delivery and
701 possible toxic effects. *Arch Toxicol* 2012, 86: 685–700.
702 Kobayashi H, Turbey B, Watanabe R, Choyke PL. Cancer Drug Delivery: Considerations in the
703 Rational Design of Nanosized Bioconjugates. *Bioconjugate Chemistry* 2014, 25: 2093−2100.

Kohler N, Sun C, Wang J, Zhang M. Methotrexate-modified superparamagnetic nanoparticles and their intracellular uptake into human cancer cells. *Langmuir* 2005, 21: 8858–8864.

Kooi ME, Cappendijk VC, Cleutjens KBJM, Kessels AGH, Kitslaar PJEHM, Borgers M, Frederick PM, Daemen MJAP, Van Engelshoven JMA. Accumulation of Ultrasmall Superparamagnetic Particles of Iron Oxide in Human Atherosclerotic Plaques Can Be Detected by In Vivo Magnetic Resonance Imaging. *Circulation* 2003, 107:2453-2458.

Kossatz S, Granke J, Couleaud P, Latorre A, Aires A, Crosbie-Staunton K, Ludwig R, Dahring H, Ettelt V, Lazzao-Carillo A, et al. Efficient treatment of breast cancer xenografts with multifunctionalized iron oxide nanoparticles combining magnetic hyperthermia and anti-cancer drug delivery. *Breast Cancer Research* 2015, 17:66.

Koziara M, Lockman PR, Allen DD, Mumper RJ. The blood-brain barrier and brain drug delivery. *J Nanosci Nanotechnol.* 2006, 6: 2712-2735.

Lee MJE, Veiseh O, Bhattarai N, Sun C, Hansen SJ, Ditzler S, Knoblaugh S, Lee D, Ellenbogen R, Zhang M, Olson JM. Rapid Pharmacokinetic and Biodistribution Studies Using Cholorotoxin-Conjugated Iron Oxide Nanoparticles: A Novel Non-Radioactive Method. *PLOS One* 2010, 5: e9536.

Leal MP, Munoz-Hernandez C, Berry C, Garcıa-Martın ML. In vivo pharmacokinetics of T_2 contrast agents based on iron oxide nanoparticles: optimization of blood circulation times. *RSC Adv.* 2015, 5: 76883–76891.

Laurent S, Forge D, Port M, Roch A, Robic C, Vander Elst L, Muller RN. Magnetic Iron Oxide Nanoparticles: Synthesis, Stabilization, Vectorization, Physicochemical Characterizations, and Biological Applications. *Chem. Rev.* 2008, 108: 2064–2110.

Longmire M, Choyke PL, Kobayashi H. Clearance Properties of Nano-sized Particles and Molecules as Imaging Agents: Considerations and Caveats. Nanomedicine 2008, 3: 703–717.

Maeda H. Tumor-Selective Delivery of Macromolecular Drugs via the EPR Effect: Background and Future Prospects. *Bioconjugate Chem.* 2010, 21: 797–802.

729 Mahmoudi M, Serpooshan V, Laurent S. Engineered nanoparticles for biomolecular imaging.
730 Nanoscale, 2011, 3, 3007-3026.
731 Maier-Hoff K, Rothe R, Scholz R, Van den Bent M.J, Taphoorn MJ, Janzer RC, Ludwin SK, Allgeier
732 A, Fisher B, Belanger K, Hau P, Brandes AA, Gijtenbeek J, Marosi C, Vecht CJ, Mokhtari K,
733 Wesseling P, Villa S, Eisenhauer E, Gorlia T, Weller M, Lacombe D, Cairncross JG, Mirimanoff RO.
734 Intracranial thermotherapy using magnetic nanoparticles combined with external beam radiotherapy:
735 Results of a feasibility study on patients with glioblastoma multiforme. *J. Neuro-Oncology* 2007, 81:
736 53-60.
737 Maier-Hoff K., Ulrich F, Nestler D, Niehoff H, Wust P, Tiesen B, Orawa H, Budach V, Jordan A.
738 Efficacy and safety of intratumoral thermotherapy using magnetic iron-oxide nanoparticles combined
739 with external beam radiotherapy on patients with recurrent glioblastoma multiforme. *J. Neuro-Oncology*
740 2011, 103: 317-324.
741 Marcus M, Karni M, Baranes K, Levy I, Alon N, Margel S, Shefi. Iron oxide nanoparticles for neuronal
742 cell applications: uptake study and magnetic manipulations. *J. Nanobiotechnol.* 2016, 14:37.
743 Mei KC, Bai J, Lorrio S, Wang JTW, Al-Jamal KT. Investigating the effect of tumor vascularization on
744 magnetic targeting *in vivo* using retrospective design of experiment. *Biomaterials* 2016, 106: 276-285.
745 Mejias R, Costo R, Roca AG, Arias CF, Veintemillas-Verdaguer S, Gonzalez-Carreno T, del Puerto
746 Morales M, Serna CJ, Manes S, Barber DF. Cytokine adsorption/release on uniform magnetic
747 nanoparticles for localized drug delivery. *J. Controlled Release* 2008, 130: 168–174.
748 Mohamaddi MR, Malkovskiy AV, Jothimuthu P, Kim KM, Parekh M, Inayathullah M, Zhuge Y,
749 Rajadas J. PEG/Dextran double layer influence Fe ion release and stability of iron oxide nanoparticles.
750 Scientific reports 2018, 8: 4286.
751 Monograph of Dexferrum, NDA 40-024/S-022, American regent inc., Shirley, NY 11967, USA.
752 Monograph of Ferhaeme, AMAG Pharmaceuticals, Inc., Lexington, MA 02421, USA.
753 Monograph of Ferrlecit 2016, Submission Control No.: 195781, Sanofi-aventis Canada, 2905 Place
754 Louis-R.-Renaud, Laval, Quebec H7V 0A3, Canada.

Monograph of Infed 2017, NDC 0023-6082-10, Allergan USA, Irvine, CA 92612, USA.

Monograph of Injectafter 2013, reference ID: 3347006. American regent, Inc. Shirley, NY 11967.

Monograph of Monofer 2017, Pharmacosmos A/S, Roervangsvej 30, DK-4300, Holbaek, Denmark.

Monograph of Venofer 2006, NDA 21-135/S-017, American regent, inc. shirley, NY 11967.

Muller EK, Grafe C, Wiekhorst F, Bergemann, Weidner A, Dutz S, Clement JH. Magnetic Nanoparticles Interact and Pass an In Vitro Co-Culture Blood-Placenta Barrier Model. *Nanomaterials* 2018, 8: 108 (doi:10.3390/nano8020108).

Ndong C, Toraya-Brown S, KekaloK, Baker I, Gerngross TU, Fiering SN, Griswold KE. Antibody-mediated targeting of iron oxide nanoparticles to the folate receptor alpha increases tumor cell association *in vitro* and *in vivo.* *International Journal of Nanomedicine* 2015, 10: 2595–2617.

Ni D, Ferreira CA, Barnhart TE, Quach V, Yu B, Jiang, D, Wei W, Liu H, Engle JW, Hu P, Cai W. Magnetic Targeting of Nanotheranostics Enhances Cerenkov Radiation-Induced Photodynamic Therapy. *J. Am. Chem. Soc.* 2018, 140: 14971−14979.

Lin MM, Kim HH, Kim H, Muhammed M, Kim DK. Iron oxide-based nanomagnets in nanomedicine: fabrication and applications. *Nano Reviews* 2010, 1: 4883 (DOI: 10.3402/nano.v1i0.4883).

Martínez-Mera I, Espinosa-Pesqueira ME, Perez-Hernadez R, Arenas-Alatorre J. Synthesis of magnetite (Fe3O4) nanoparticles without surfactants at room temperature. *Materials Letters* 2007, 61: 4447–4451.

Obaidat IM, Issa B, Haik Y. Magnetic properties of Magnetic Nanoparticles for efficient Hyperthermia. *Nanomaterials* 2015, 5: 68-89.

Ohno K, Mori C, Akashi T, Yoshida S, Tago Y, Tsujii Y, Tabata Y. Fabrication of Contrast Agents for Magnetic Resonance Imaging from Polymer-Brush-Afforded Iron Oxide Magnetic Nanoparticles Prepared by Surface-Initiated Living Radical Polymerization. *Biomacromolecules* 2013, 14: 3453−3462.

Osborne EA, Atkins TM, Gilbert DA, Kauzlarich SM, Liu K, Louie AY. Rapid Microwave-Assisted Synthesis of Dextran-Coated Iron Oxide Nanoparticles for Magnetic Resonance Imaging. *Nanotechnology* 2012, 23: 215602.

781 Osuna J, Caro D, Amiens C, Chaudret B. Synthesis, Characterization, and Magnetic Properties of
782 Cobalt Nanoparticles from an Organometallic Precursor. *J. Phys. Chem.* 1996, 100: 14571–14574.
783 Parat A, Kryza D, Degoul F, Taleb J, Viallard C, Janier M, Garofalo A, Bonazza P, Heinrich-Balard L,
784 Cohen R, Miot-Noirault E, Chezal J-M, Billoteycg C, Felder-Flesch D. Radiolabeled dendritic probes as
785 tools for high in vivo tumor targeting: application to melanoma. *J. Mat. Chem. B.* 2015, 3: 2560-1571.
786 Park JH, Maltzahn G, Zhang L, Schwartz M, Ruoslati E, Bhatia SN, Sailor MJ. Magnetic Iron Oxide
787 Nanoworms for Tumor Targeting and Imaging. *Adv Mater.* 2008, 20: 1630–1635.
788 Park J, Cho W, Park HJ, Cha KH, Ha DC, Choi YW, Lee HY, Cho SH, Hwang SJ. Biodistribution of
789 newly synthesized PHEA-based polymer-coated SPION in Sprague Dawley rats as magnetic resonance
790 contrast agent. *International Journal of Nanomedicine* 2013, 8: 4077–4089.
791 Peng X-H, Qian X, Mao H, Wang AY, Chan Z, Nie S, Shin DM. Targeted magnetic iron oxide
792 nanoparticles for tumor imaging and therapy. *International Journal of Nanomedicine* 2008, 3: 311–
793 321.
794 Périgo EA, Hemery G, Sandre O, Ortega D, Garaio E, Plazaola F, Teran FJ. Fundamentals and advances
795 in magnetic hyperthermia. *Appl. Phys. Rev.* 2015, 2: 041302.
796 Pham BTT, Colvin EK, Pham NTH, Kim BJ, Fuller ES, Moon EA, Barbey R, Yuen S, Rickman BH,
797 Bryce NS, Bickley S, Tanudji M, Jones SK, Howell VM, Hawkett BS. Biodistribution and Clearance of
798 Stable Superparamagnetic Maghemite Iron Oxide Nanoparticles in Mice Following Intraperitoneal
799 Administration. *Int. J. Mol. Sci.* 2018, 19: 205 (doi:10.3390/ijms19010205).
800 Phu ND, Ngo DT, Hoang LH, Luong N. H. Crystallization process and magnetic properties of
801 amorphous iron oxide nanoparticles. *Journal of Physics D: Applied Physics.* 2011, 44: 345002.
802 Prabu P, Vedakumari WS, Sastry TP. Time-dependent biodistribution, clearance and biocompatibility of
803 magnetic fibrin nanoparticles: an *in vivo* study. *Nanoscale* 2015, 7: 9676-9685.
804 Qian X, Han X, Chen Y. Insights into the unique functionality of inorganic micro/nanoparticles for
805 versatile ultrasound theranostics. *Biomaterials* 2017, 142: 13-30.

Quan Q, Xie J, Gao H, Yang M, Zhang F, Liu G, Lin X, Wang, A, Eden HS, Lee S, Zhang G, Chen X. HSA Coated Iron Oxide Nanoparticles as Drug Delivery Vehicles for Cancer Therapy. *Mol. Pharmaceutics* 2011, 8: 1669–1676.

Ramimoghadam D, Bagheri S, Hamid SBA. Progress in electrochemical synthesis of magnetic iron oxide nanoparticles. *Journal of Magnetism and Magnetic Materials* 2014, 368: 207–229.

Rao L, Bu LL, Xu JH, Cai B, Yu GT, Yu X, He Z, Huang Q, Li A, Guo SS, Zhang WF, Liu W, Sun ZJ, Wang H, Wang TH, Zhao XZ. Red Blood Cell Membrane as a Biomimetic Nanocoating for Prolonged Circulation Time and Reduced Accelerated Blood Clearance. *Small* 2015, 11: 6225–6236.

Reddy LH, Sharma RK, Chuttani K, Mishra AK, Murthy RSR. Influence of administration route on tumor uptake and biodistribution of etoposide loaded solid lipid nanoparticles in Dalton's lymphoma tumor bearing mice. *Journal of Controlled Release* 2005, 105: 185–198.

Remya NS, Syama S, Sabareeswaran A, Mohanan PV. Toxicity, toxicokinetics and biodistribution of dextran stabilized Iron oxide Nanoparticles for biomedical applications. *International Journal of Pharmaceutics* 2016, 511: 586–598.

Ruiz A, Hernandez Y, Cabal C, Gonzalez E, Veintemillas-Verdaguer S, Martınezc E, Morales MP. Biodistribution and pharmacokinetics of uniform magnetite nanoparticles chemically modified with polyethylene glycol. *Nanoscale* 2013, 5: 11400-11408.

Ruiz A, Gutiérrez L, Cáceres-Vélez PR, Santos D, Chaves SB, Fascineli ML, Garcia MP, Azevedoc RB, Morales MP. Biotransformation of magnetic nanoparticles as a function of coating in a rat model. *Nanoscale* 2015, 7: 16321-16329.

Sakulkhua U, Mahmoudib M, Maurizia L, Coullereza G, Hofmann-Amtenbrink M, Rezaeee F, Motazacker M, Vriese M, Hofmanna H. Significance of surface charge and shell material of Superparamagnetic Iron Oxide Nanoparticles (SPIONs) based core/shell nanoparticles on the composition of the protein corona. *Biomater. Sci.* 2015, 3: 265-278.

Sahoo Y, Goodarzi A, Swihart MT, Ohulchanskyy TY, Kaur N, Furlani EP, Prasad P. Aqueous Ferrofluid of Magnetite Nanoparticles: Fluorescence Labeling and Magnetophoretic Control. *J. Phys. Chem. B* 2005, 109: 3879-3885.

Sakulkhu U, Mahmoudi M, Maurizi L, Salaklang J, Hofmann H. Protein Corona Composition of Superparamagnetic Iron Oxide Nanoparticles with Various Physico-Chemical Properties and Coatings. *Scientific reports*, 4: 5020 (doi: 10.1038/srep05020).

Salazar-Alvarez G, Muhammed M, Zagorodni AA. Novel flow injection synthesis of iron oxide nanoparticles with narrow size distribution, *Chemical Engineering Science* 2006, 61: 4625-4633.

Salimi M, Sarkar S, Fathi S, Alizadeh AM, Saber R, Moradi F, Delavari H. Biodistribution, pharmacokinetics, and toxicity of dendrimer-coated iron oxide nanoparticles in BAL B/c mice. *International Journal of Nanomedicine* 2018, 13: 1483–1493.

Santoyo Salazar J, Perez L, Abril O, Phuoc LT, Ihiawakrim D, Vazquez M, Greneche JM, Begin-Colin S, Pourroy G. Magnetic Iron Oxide Nanoparticles in 10-40 nm Range: Composition in Terms of Magnetite/Maghemite Ratio and Effect on the Magnetic Properties. *Chem. Mater*. 2011, 23: 1379–1386.

Santra S, Kaittanis C, Perez JM. Cytochrome c encapsulating theranostic nanoparticles: A novel bifunctional system for targeted delivery of therapeutic membrane impermeable proteins to tumors and imaging of cancer therapy. *Mol. Pharmaceutics* 2010, 7: 1209–1222.

Schleich N, Po C, Jacobs D, Ucakar B, Gallez B, Danhier F, Préat V. Comparison of active, passive and magnetic targeting to tumors of multifunctional paclitaxel/SPIO-loaded nanoparticles for tumor imaging and therapy. *Journal of Controlled Release* 2014, 194: 82–91.

Shanehsazzadeh , Oghabian MA, Daha FJ, Amanlou M, Allen BJ. Biodistribution of ultra small superparamagnetic iron oxide nanoparticles in BALB mice. *J Radioanal Nucl Chem* 2013, 295:1517–1523.

Shen CC, Wang CC, Liao MH, Jan TR. A single exposure to iron oxide nanoparticles attenuates antigen-specific antibody production and T-cell reactivity in ovalbumin-sensitized BALB/c mice. *International Journal of Nanomedicine* 2011, 6: 1229–1235.

Simberg D, Park JH, Karmali PD, Zhang WM, Merkulov S, McCrae K, Bhatia SN, Sailor M, Ruoslahti E. Differential proteomics analysis of the surface heterogeneity of dextran iron oxide nanoparticles and the implications for their in vivo clearance. *Biomaterials* 2009, 30: 3926–3933.

Singh N, Jenkins GJS, Asadi R, Doak SH. Potential toxicity of superparamagnetic iron oxide nanoparticles (SPION). *Nano Reviews* 2010, 1: 5358 (DOI: 10.3402/nano.v1i0.5358).

Soenen SJH, Nuytten N, De Meyer SF, De Smedt SC, De Cuyper M. High Intracellular Iron Oxide Nanoparticle Concentrations Affect Cellular Cytoskeleton and Focal Adhesion Kinase-Mediated Signaling. Small 2010, 6: 832–842.

Sonmez E, Aydin E, Turkez H, Özbek E, Togar B, Meral K, Çetin D, Cacciatore I, Di Stefano A. Cytotoxicity and genotoxicity of iron oxide nanoparticles: an in vitro biosafety study. *Arch. Biol. Sci.* 2016, 68: 41-50.

Stepien G, Moros M, Pérez-Hernández M, Monge M, Gutiérrez L, Fratila RM, De las Heras M, Guillén SM, Lanzarote JJP, Solans C, Pardo J, De la Fuente JM. Effect of Surface Chemistry and Associated Protein Corona on the Long-Term Biodegradation of Iron Oxide Nanoparticles In Vivo. *ACS Appl. Mater. Interfaces* 2018, 10: 4548−4560.

Strehl C, Schellmann S, Maurizi L, Hofmann-Amtenbrink M, Häupla T, Hofmann H, Buttgereit F, Gabera T. Effects of PVA-coated nanoparticles on human T helper cell activity. *Toxicology Letters* 2016, 245: 52–58.

Sun Y, Duan L, Guo Z, DuanMu Y, Ma M, Xu L, Zhang Y, Gu N. An improved way to prepare superparamagnetic magnetite-silica core-shell nanoparticles for possible biological application. *Journal of Magnetism and Magnetic Materials* 2005, 285: 65–70.

Sun J, Wang S, Zhao, D, Han Hun F, Weng L, Liu H. Cytotoxicity, permeability, and inflammation of metal oxide nanoparticles in human cardiac microvascular endothelial cells. *Cell Biol Toxicol* 2011, 27: 333–342.

Sun T, Zhang YS, Pang B, Hyun DC, Yang M, Xia Y. Engineered Nanoparticles for Drug Delivery in Cancer Therapy. *Angew. Chem. Int. Ed.* 2014, 53: 12320-12364.

Sun Z, Worden M, Thliveris JA, Hombach-Klonisch S, Klonisch T, Van Lierop J, Hegmann T, Miller DW. Biodistribution of negatively charged iron oxide nanoparticles (IONPs) in mice and enhanced brain delivery using lysophosphatidic acid (LPA). *Nanomedicine: Nanotechnology, Biology, and Medicine* 2016, 12: 1775–1784.

Thorek DLJ, Chen AK, Czupryna J, Tsourkas A. Superparamagnetic Iron Oxide Nanoparticle Probes for Molecular Imaging. *Annals of Biomedical Engineering* 2006, 34: 23-38.

Tietze R, Lyer S, Durr S, Struffert T, Engelhorn T, Schwarz M, Eckert E, Göen T, Vasylyev S, Peukert W, Wiekhorst F, Trahms L, Dörfler A, Alexiou C, Efficient drug-delivery using magnetic nanoparticles–biodistribution and therapeutic effects in tumour bearing rabbits. *Nanomedicine* 2013, 9: 961–971.

Treuel L, Jiang X, Nienhaus GU. New views on cellular uptake and trafficking of manufactured nanoparticles. *J R Soc Interface* 2013, 10: 20120939.

Utani K-I, Kohno Y, Okamoto A, Shimizu N. Emergence of Micronuclei and Their Effects on the Fate of Cells under Replication Stress. Plos One 2010, 5: e10089.

Veiseh O, Gunn J, Zhang M. Design and fabrication of magnetic nanoparticles for targeted drug delivery and imaging. *Adv Drug Deliv Rev.* 2010, 62: 284–304.

Veintemillas-Verdaguer S, Morales MP, Serna SJ. Continuous production of γ-Fe O ultrafine powders by laser pyrolysis. *Materials Letters* 1998, 35: 227-231.

Veiseh O, Sun C, Fang C, Bhattarai N, Gunn J, Kievit F, Du K, Pullar B, Lee D, Ellenbogen RG, Olson J, Zhang M. Specific targeting of brain tumors with an optical/magnetic resonance imaging nanoprobe across the blood-brain barrier. *Cancer Res.* 2009, 69: 6200–6207.

Walter A, Billotey C, Garofalo A, Ulhaq-Bouillet C, Lefèvre C, Taleb J, Laurent S, Vander Elst L, Muller RN, Lartigue L, Gazeau F, Felder-Flesch D, Begin-Colin S. Mastering the Shape and Composition of Dendronized Iron Oxide Nanoparticles To Tailor Magnetic Resonance Imaging and Hyperthermia. *Chem. Mat.* 2014, 26: 5252−5264.

907 Wan J, Chen X, Wang Z, Yang X, Qian Y. A soft-template-assisted hydrothermal approach to single-
908 crystal Fe_3O_4 nanorods. *Journal of Crystal Growth* 2005, 276: 571-576.
909 Wang J, Chen Y, Chen B, Ding J, Xia G, Gao C, Cheng J, Jin N, Zhou Y, Li X, Tang M, Wang XM.
910 Pharmacokinetic parameters and tissue distribution of magnetic Fe_3O_4 nanoparticles in mice.
911 *International Journal of Nanomedicine* 2010, 5: 861–866.
912 Wang L, Huang J, Chen H, Wu H, Xu Y, Li Y, Yi H, Wang YA, Yang L, Mao H. Exerting Enhanced
913 Permeability and Retention Effect Driven Delivery by Ultrafine Iron Oxide Nanoparticles with T1–T2
914 Switchable Magnetic Resonance Imaging Contrast. *ACS Nano* 2017, 11: 4582–4592.
915 Wei H, Brunsa OT, Kaulb MG, Hansen EC, Barch M, Wisniowska A, Chen O, Chen O, Li N, Okada S,
916 Cordero JM, Heine M, Farrar CT, Montanaa DM, Adamb G, Ittrich H, Jasanoff A,, Nielsen P, Bawendi
917 MG. Exceedingly small iron oxide nanoparticles as positive MRI contrast agents. *PNAS* 2017, 114:
918 2325–2330.
919 Wu W, He Q, Jiang C. Magnetic Iron Oxide Nanoparticles: Synthesis and Surface Functionalization
920 Strategies. *Nanoscale Res Lett* 2008, 3:397–415.
921 Wu W, Wu Z, Yu T, Jiang C, Kim WS. Recent progress on magnetic iron oxide nanoparticles:
922 synthesis, surface functional strategies and biomedical applications. *Sci. Technol. Adv. Mater.* 2015,
923 16: 023501.
924 Xie Y, Liu, D, Cai, C, Chen X, Zhou Y, Wu L, Sun Y, Dai H, Kong X, Liu P. Size-dependent
925 cytotoxicity of Fe_3O_4 nanoparticles induced by biphasic regulation of oxidative stress in different human
926 hepatoma cells. *International Journal of Nanomedicine* 2016, 11: 3557–3570.
927 Xu C, Shi S, Feng L, Chen F, Graves SA, Ehlerding EB, Goel S, Sun H, England CG, Nickles RJ, Liu
928 Z, Wang T, Cai W. Long circulating reduced graphene oxide–iron oxide nanoparticles for efficient
929 tumor targeting and multimodality imaging. *Nanoscale*, 2016, 8: 12683–12692.
930 Wang YXJ, Xuan S, Port M, Idee JM. Recent Advances in Superparamagnetic Iron Oxide Nanoparticles
931 for Cellular Imaging and Targeted Therapy Research. *Current Pharmaceutical Design* 2013, 19: 6575-
932 6593.

933 Wang H, Mua Q, Reviaa R, Wanga K, Tiand B, Lina G, Leec W, Hong Y-K, Zhanga M. Iron oxide-
934 carbon core-shell nanoparticles for dual-modal imaging-guided photothermal therapy. *Journal of*
935 *Controlled Release* 2018, 289: 70–78.
936 Wilhelm S, Tavares AJ, Dai Q, Ohta S, Audet J, Dvorak HF, Chan WCW. Analysis of nanoparticle
937 delivery to tumours. Nature Reviews Materials 2016, 1:1-12.
938 Yang L,Guo G, Niu XY, Liu J. Dendritic Cell-Based Immunotherapy Treatment for Glioblastoma
939 Multiforme. *BioMed Research International* 2015, article ID 717530.
940 Yang L, Kuang H, Zhang W, Aguilar ZP, Xiong Y, Lai W, Xu H, Wei H. Size dependent
941 biodistribution and toxicokinetics of iron oxide magnetic nanoparticles in mice. *Nanoscale* 2015, 7:
942 625–636.
943 Yang X, Hong H, Grailer JJ, Rowland IJ, Javadi A, Hurley SA, Xiao Y, Yang Y, Zhang Y, Nickles RJ,
944 Cai W, Steeber DA, Gong S. cRGD-functionalized, DOX-conjugated, and ^{64}Cu-labeled
945 superparamagnetic iron oxide nanoparticles for targeted anticancer drug delivery and PET/MR imaging.
946 *Biomaterials* 2011, 32: 4151-4160.
947 Yu J, Yin W, Zheng X, Tian G, Zhang X, Bao T, Dong X, Wang Z, Gu Z, Ma X, Zhao Y. Smart
948 MoS_2/Fe_3O_4 Nanotheranostic for Magnetically Targeted Photothermal Therapy Guided by Magnetic
949 Resonance/Photoacoustic Imaging. Theranostics 2015, 5: 931-945.
950 Zadnik PL, Molina CA, Sarabia-Estrada R, Groves ML, Wablbler M, Mihalic J, McCarthy EF,
951 Gokaslslan ZL, Ivkov R, Sciubbbba, DM. Characterization of intratumor magnetic nanoparticle
952 distribution and heating in a rat model of metastatic spine disease. *J Neurosurg Spine* 2014, 20:740-
953 750.
954 Zhao Z, Zhou Z, Bao J, Wang Z, Hu J, Chi X, Ni K, Wang R, Chen X, Chen Z, Gao J. Octapod iron
955 oxide nanoparticles as high performance T_2 contrast agents for magnetic resonance imaging. *Nature*
956 *communications* 2013, 4:2266 (DOI: 10.1038/ncomms3266).

957 Zhang C, Liu H, Cui Y, Li X, Zhang Z, Zhang Y, Wang D. Molecular magnetic resonance imaging of
958 activated hepatic stellate cells with ultrasmall superparamagnetic iron oxide targeting integrin $\alpha v\beta_3$ for
959 staging liver fibrosis in rat model. *International Journal of Nanomedicine* 2016, 11: 1097–1108.
960 Zhen G, Muir BW, Moffat BA, Harbour P, Murray KS, Moubaraki B, Suzuki K, Madsen I, Agron-
961 Olshina N, Waddington L, Mulvaney L, Hartley PG. Comparative Study of the Magnetic Behavior of
962 Spherical and Cubic Superparamagnetic Iron Oxide Nanoparticles. *J. Phys. Chem. C* 2011, 115, 327-
963 334.
964 Zhou J, Zhang J, Gao W. Enhanced and selective delivery of enzyme therapy to 9L-glioma tumor via
965 magnetic targeting of PEG-modified, β-glucosidase-conjugated iron oxide nanoparticles. *International*
966 *Journal of Nanomedicine* 2014, 9: 2905–2917.
967 Zhu X, Tian S, Cai Z. Toxicity Assessment of Iron Oxide Nanoparticles in Zebrafish (Danio rerio) Early
968 Life Stages. *Plos One* 2012, 7: e46286.
969 Zolata H, Davani FA, Afarideh H. Synthesis, characterization and theranostic evaluation of Indium-111
970 labeled multifunctional superparamagnetic iron oxide nanoparticles. *Nuclear Medicine and Biology*
971 2015, 42: 164–170.

FIGURES:

Figure 1: A schematic picture representing two different types of applications of iron oxide nanoparticles for treatments of iron anemia disease and cancer.

Figure 2: The different properties of iron oxide nanoparticle properties influencing their biodistribution.

TABLE:

Table 1: Commercialized or CE marked iron oxide nanoparticles for treatments of iron anemia disease and glioblastoma.

Table 2: Biodistribution properties and pharmacodynamics parameters of various iron oxide nanoparticles.

Table 3: Percentage of injected IONP ending up in tumor through the EPR effects when different quantities of IONP are administered intravenously to mice or rats bearing different types of tumors.

Table 4: Percentage of injected IONP ending up in tumor through molecular targeting when different quantities of IONP conjugated to various targeting agents are administered intravenously to mice bearing different types of tumors.

Table 5: Percentage of injected IONP ending up in tumor through magnetic targeting targeting when different quantities of IONP are administered intravenously to mice bearing different types of tumors and the tumor is exposed to a magnetic field of various strengths.

990

Two medical applications of iron oxide nanoparticles

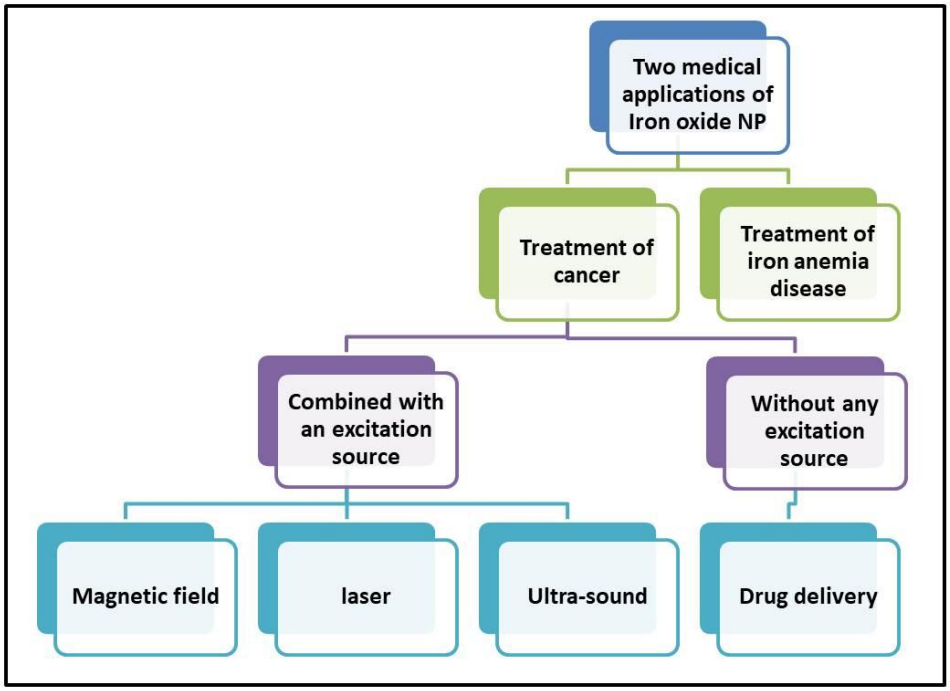

Figure 1

991

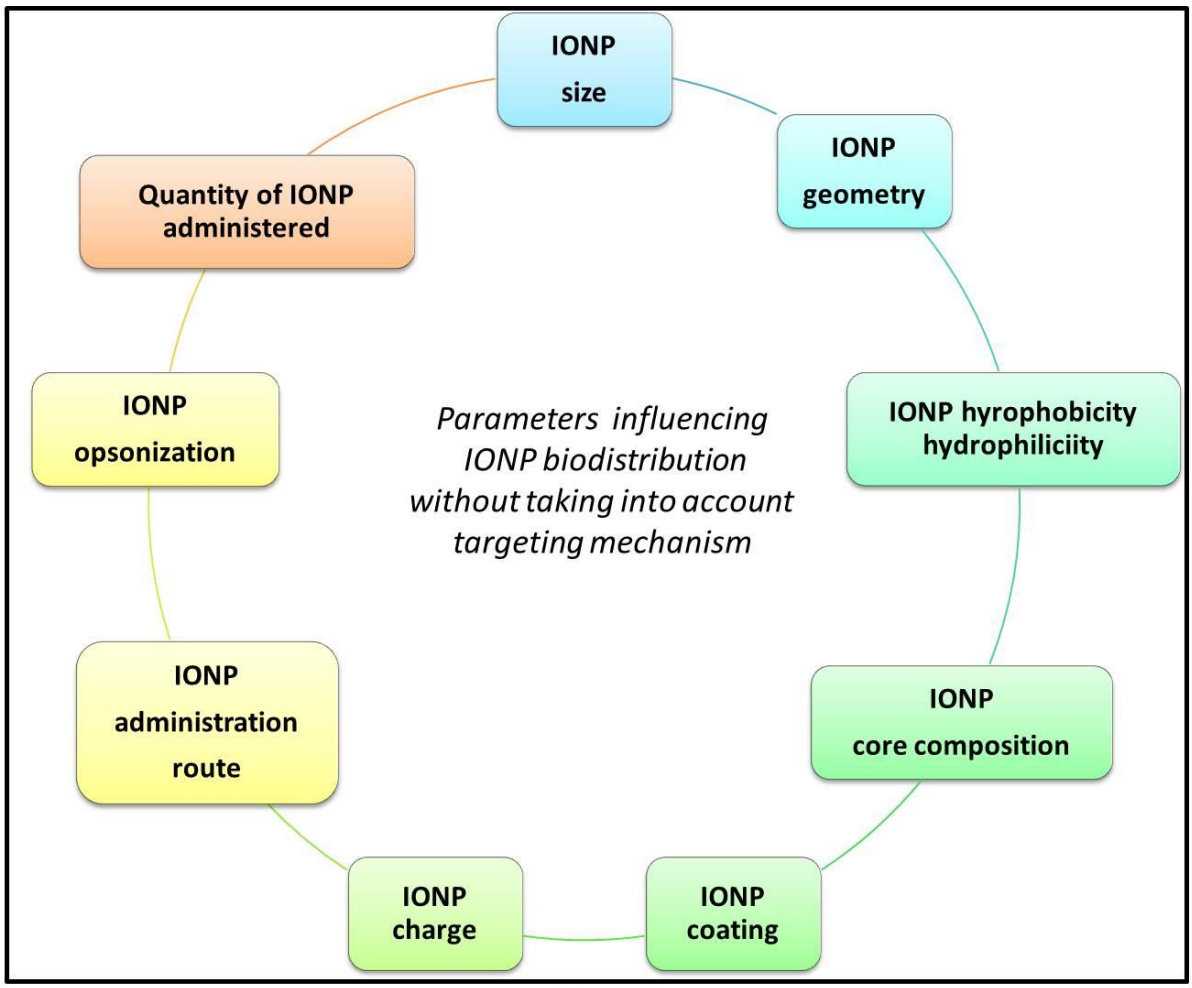

Figure 2

992

993

994

995

Product name	Product type	Status	Application
Feraheme, Ferumoxytol, Rienso	FeOCHONa NP + polyglucose sorbitol carboxymethyl ether coating	Commercialized	Treatment of IDA in patients with CKD
Ferrisat	Iron + Dextran	Commercialized	Treatment of IDA
Venofer	Iron + sucrose	Commercialized	Treatment of IDA in patients with CKD
DexFerrum, iron dextran injection	Iron + dextran	Commercialized	Treatment of IDA in patients with CKD
Injectafter Ferinject	Sodium ferric gluconate	Commercialized	Treatment of IDA in patients with CKD
Nanotherm	amino-silane coated iron oxide nanoparticle	Commercialized	Magnetic hyperthermia treatment

Table 1

996

997

Biodistribution/pharmacodynamic parameters of $Fe_3O_4/\gamma Fe_2O_3$ NP

NP size (nm) name	Coating type	Quant. Admin.	Admin. Route	Animal	Organs with large NP accumulation	Organs with low NP accumulation	Elimination route	Pharma. paramet.	Remarks	Ref (first aut. name/year pub.)
5, 15, 30 (TEM) 13, 30, 50 (hydro)	PEG	5 mg/kg	iv	Mice	Liver, spleen (24h)	Lung, kifney, brain (24h)	Liver and spleen Degraded products in blood	$t_{1/2}$ = 200 min (5 nm) $t_{1/2}$ = 63 min (30 nm)	Decrease in half life with increasing sizes	Gu2012
12-15	DMSA	0.5-2 mg/kg	iv	pig	Liver, spleen	Lungs,	Liver (no accumulation in kidney)	$t_{1/2}$ = 15 min.	Decrease in blood pressure after NP admin.	Edge2016
11	OA + pluronic	10 mg/kg	iv	Rats	Liver, spleen	Brain, heart, kidney, lung	18-22% of NP through urine and feces during 7 weeks	Clearance > 3 weeks	None	Jain 2008
17-46 (hydro)	PEG1500-PEG800	5 mg/kg	iv	mice	Liver, kidney (0-50 h. after amin.)	Bladder, muscle (0-50 h)	Through Liver Renal clerance	NA	Very different biodistribution profile compared with Gd	Leal 2015
32-46 (hydro)	PEG Dextran	100 mg/kg	iv	mice	Liver, spleen (24 h. after inj)	NA	Spleen and/or liver	$t_{1/2}$ < 1h	NP in blood during 24 h.	Mohamaddi 2018
10-25	PEG	90 mg/kg	ip	Mice (ovarian tumor)	Liver, spleen, omentum, mesentery (0-1 week)	Bladder, brain, colon, heart, left kidney, left ovary, lungs, peritoneum, stomach, uterus	Excretion in feces (1h-1 week) Spleen and liver macrophages	NA	More NP in tumor for larger SPION (1-24 h after admin.)	Pham 2018
25	Dextran	300-2000 mg/kg	iv	Mice	Liver, Spleen	kidney	lack of defined pathway for excretion	NA	Iron accumulation in liver, spleen, kidney does not induce tox.	Remya 2016
12	PEG	2.5-5 mg/kg	iv	Rats	Liver (3 h)	Spleen, lung (3 h)	Liver assimilation of iron Excretion from liver in 200 h.	$t_{1/2}$ = 20 min	NP excreted in the form of free iron.	Ruiz 2013
10 (TEM)	dendrimer	250 mg/kg	ip	Mice (tumor)	Liver, lung, heart, kidney, tumor, heart (4-24 h)	NA	Excretion through kidney and absorption in lungs	$t_{1/2}$ < 24h	Unusual mode of excretion	Salimi2018
41 (hydro)	dextran	50 mg/kg	iv	Mice	Liver (< 24h) Heart (< 5 min) Lung (<60 min)	Kidney, adrenal, pancreas, tail, carcass	Feces excretion negligible. NP accumulate in liver + spleen	$t_{1/2}$ < 5 min	Gradual increase of NP accumulation in spleen (peak at 60 min)	Shanehsazzadeh 2013
29 (hydro)	EDT Ethylenediami-netriacetate		iv	Mice	Liver (< 30 min)	Spleen, kidney (<30 min)	Essentially liver (possibly a little bit through kidney)	$t_{1/2}$ = 6 min	Can cross the BBB due to the coating LPA	Sun2016
20 (TEM)	None	600 mg/kg	Intra-gastric	Mice	Liver, Spleen (> 10 days)	Heart, lungs, kidneys, brain, stomac, small intestine (> 10 days)	Renal excretion modest	$t_{1/2}$ > 10 days	IONP can cross the BBB	Wang2011
2.5-7 (TEM)	ZDS Zwitterionic dopmanie sulfonate	12 mg/kg	iv	Mice	Liver, carcass	GIT, Kidney, Spleen, lung, heart, tail (24 h)	After 24 h, majority of iron from NP in urines	NA	Renal clearance due to small size of IONP	Wei2017
20 (TEM)	NA	600 mg/Kg	Intra-gastric	Mice	Liver, spleen	Heat, lungs, kidney, brain, stomach, small intestine	Modest renal excretion	NA	Presence of IONP in all organs	Wang2010
10, 20, 30, 40	carboxyl	20 mg/Kg	iv	Mice	10 nm IONP: liver 40 nm IONP: Spleen	stomach, intestine, and uterus	All IONP in Feces Small IONP (10 nm) in urine	NA	Biodistribution and elimination depends on size of IONP	Yang2015

Table 2-1

998

IONP size (nm) name	Not Fe203 Coating / drug	Quant. Admin.	Admin. Route	Animal	Organ with larger NP accumulation	Organs with lower NP accumulation	Elimination route	Pharma. paramet.	Remarks	Ref (first aut. name/year pub.)
20 (TEM)	PEG	10 mg/kg	iv	Mice	Liver, spleen (24h, 72h)	Kidney (24h, 72h)	NA	NA	NA	Arami 2015
NA	Chitosan + Cholorotoxin (targeting)	10 mg/kg	iv	Mice	Liver, spleen, kidney (0-48h) No diff. with/without targeting	Colon, brain, heart, lung, pancreas, muscle, small intestine, gonad, bone marrow (0-48h) No diff with/without targeting	Kidney and liver	$t_{1/2}$ = 8 h (with targeting) $t_{1/2}$ = 7 h (without targeting)	Longer circulation with targeting molecule that prevents elimination.	Lee 2010
5 (TEM) 10-20 (hydro)	PEG RGD-modified	5 mg/Kg	iv	Mice bearing HepG2 tumor	Liver, spleen (not a big difference between blank, PEG, RGD-modified)	Heart, lung, kidney, tumor	liver	$t_{1/2}$ = 92 min (RGD)	For heart, liver, spleen, lung, kidney): No difference in biidostribution between blank, PEG-IONP or RGD-IONP For tumor: No difference between IONP-RGD and IONP-PEG	Jia2016
120 (hydro)	DOXO + RGD (targeted) DOXO (non-targeted)	0.5 mg/Kg	iv	Mice bearing CNS-1 GBM	Non-targeted organ: distribution in liver, spleen, heart, brain, kidney		Organs of the RES	NA	Non-targeted IONP: 2% in tumor Targeted IONP: 4.5% in tumor	Karathanasis2016
8-10 (TEM) 66 (hydro)	PHEA	1 mg/Kg	iv	Rats	liver	Spleen, lung, kidney, small intestine	Liver (faces excretion) Kidney (urine excretion)	$t_{1/2}$ = 15-24 min (blood). $t_{1/2}$ = 6-20 days (liver)	IONP laneled with 59Fe eliminated by kidney and faces IONP labeled with 14C eliminated by faces	Park2013
Resovist 65 (hydro)	Dextran ± fucoidan	2 mg/kg	iv	Mice bearing GL261 tumor	Liver, blood, spleen	Heart, kidney	Liver + kidney (w fucoidan) Liver (wo fucoidan)	$t_{1/2}$ = 37 min w/o fucoidan $t_{1/2}$ = 150 min w fucoidan	With fucoidan, two times more IONP in the tumor	Abdollah2018
18	Rituximab	6.4 mg/kg	iv	Mice bearing CD-20 tumor	Liver, spleen, kidney, blood, tumor, stomach (time dependent) % tumor = 9 % ID/g.	Intestine, muscle	NA	NA	Compartive kinetics for different organs: IONP in Lung, kidney, spleen, liver, intestine, stomac: ↗ during 5-15 h then ↘ IONP in blood, heart : gradual decrease IONP in tumor: gradual increase	Azadkbakht2018
10 (TEM) 47 (hydro)	Polyacrylic acid	8, 20, 50 mg/kg	iv	Mice	Liver, spleen (dose dependant)	Lung, heart, tail	NA	NA	Accumulation in liver and spleen increases with increasing quantity of IONP administered	Couto2016
20	PEGMA (LMW = 14 000 and HMW = 130 000)	50 mg/Kg	iv	Mice	LMW: Spleen, liver, lung HMW: heart, lung, thymus, liver, spleen, kidney, tumor	LMW: Heart, thymus, kidney, tumor HMW: none	NA	$t_{1/2}$ = 24h (HMW) $t_{1/2}$ < 2h (LMW)	Much longer circulation time and higher accumulation ifn tumor for HMW than LMW	Ohno2013
26 (hydro)	fibrin	5 mg/Kg	iv	Mice	Liver	Spleen, lung, kidney, heart	Urine and feces	$t_{1/2}$ = 12 hours	Accumulation of IONP in liver and progressive departure of IONP from liver between 6h and 28d	Prabu2015
41 (hydro)	Dextran + DOTA	4 mg/Kg	iv	Mice with breast tumor	Blood, liver, tumor	Kidney, stomach, intestine, colon, heart, lung, bone	NA	NA	Between 4h and 24hpost inject., IONP leave blood and remain in liver and tumor % ID in tumor = 0.25 %	Rasaneh2015
12	Glucose or PEG	6 mg/kg	iv	Mice	Liver, spleen	NA	NA	NA	Accelerated degradation and clerance with PEG compared with glucose	Stepien2018

Table 2-2

999

EPR targeting of tumors with different types of iron oxyde nanoparticle

IONP type / size	Admin. Route	Quantity admin.	Tumor volume Tumor weight	Tumor type	Percentage of injected dose per gram of tumor	Percentage of IONP in tumor (% ID)	Ref.
SPION encapsulated in nanocapsule	iv	2 mg (mice)	100 mm^3 0.2 g	CT-26 colon tumor	2%	0.2%	Al-Jamal2016
G100 starch coated IONP (Chemicell)	iv	1.7 mg (rats)	50-70 mm^3 0.1 g	9L glioma	5.10^{-3} %	5.10^{-4} %	Chertok2007
IONP of 30 nm	iv	2 mg (mice)	100-200 mm^3 0.2 g	BT-474 breast cancer cells	7%	1.4%	Dong2015
IONP of 100 nm	iv	2 mg (mice)	100-200 mm^3 0.2 g	BT-474 breast cancer cells	0.75-1.25%	0.15-0.25%	Dong2015
SPIO (6-10 nm) (Taiwan advanced Nanotech)	iv	300 µg (rats)	20 mm^3 0.1 g	C6 glioma	1%	0.1 %	Fan2013
SPION with amino groups (36 nm)	iv	4 mg (rats)	23 mm^3 0.1 g	C6 glioma	0.1%	0.01%	Fan2016
SPION embedded nanobubbles	iv	3 mg (rats)	100 mm^3 0.2 g	Glioma tumor	3%	0.6%	Huang2013
SPION (10 nm) in nanocapsule	iv	1.4 mg (mice)	400 -600 mm^3 0.5 g	CT26 4T1 LLC B16F10	2.5% (CT26) 2% (4T1) 1% (LLC) 2% (B16F10)	1.25% (CT26) 1% (4T1) 0.5% (LLC) 1% (BL6F10)	Mei2016
SPION (ZnMnFeO)	iv	0.8 mg (mice)	150 mm^3 0.2 g	4T1 tumor	5%	1%	Ni2018
IONP (240 nm) IONP + Paclitaxel (240 nm)	iv	0.2-0.5 mg (mice)	50-100 mm^3 0.1-0.2 g	CT26	NA	0.1% (SPION) 0.1% (SPION+ Paclitaxel)	Schleich2014
SPION + PEG (7 nm) SPION + two PEG (7 nm)	iv	0.125 mg (mice)	100 mm^3 0.2 g	4T1	8% (IONP + PEG) 15% (IONP + 2 PEG)	1.6% (IONP + PEG) 3% (IONP + 2 PEG)	Xu2016
Starch coated D-MNP (Chemicell) conjugated with PEG and β-glucosidase	Iv	0.24 mg (mice)	300-400 mm^3 0.4 g	9L glioma	1%	0.4%	Zhou2014
Starch coated D-MNP (Chemicell) conjugated with β-glucosidase	Iv	0.24 mg (mice)	300-400 mm^3 0.4 g	9L glioma	0.5%	0.2%	Zhou2014
Starch coated D-MNP (Chemicell)	iv	0.24 mg (mice)	300-400 mm^3 0.4 g	9L glioma	0.1%	0.04%	Zhou2014

Table 3

1000

Molecular targeting of tumors with different types of iron oxyde nanoparticles

IONP type ± targeting agent (TA)	Admin. Route	Quantity admin.	Molecular targeting (MDT)	Type of targeted tumor	Tumor volume/ Weight	Percentage of injected dose per gram of tumor (%ID/g of tumor)	Percentage of IONP in tumor (% ID)	Ref.
SPION (BNF) + PSMA antibody (with TA)	iv	0.25-4 mg (mice)	PSMA antibody Targets PSMA	PC3 prostate tumor	140 mm^3 0.2 g	2.9% (with TA)	0.6% (with TA)	Azad2015
SPION (BNF) + anti-GD2 antibody (with TA)	iv	0.073 mg (mice)	GD2 expressed on CHLA-20 neuroblastoma	CHLA-20 neuroblastoma Xenografts	NA	5.7% (with TA) 0% (without TA)	NA	Baiu2015
SPION + Biotin (with TA)	iv	NA	Targets avidin injected in the tumor	NA	130 mm^3 0.2 g	0.6% (with TA)	0.1% (with TA)	Chauhan 2013a
SPION + folate (with TA)	iv	NA	Targets folate receptors of KB cancer cells	KB cells	1.6 cm^3 1.9 g	0.2-0.6% (with TA)	0.38-1.14% (with TA)	Chauhan 2013b
IONP of 30 nm (without TA) IONP of 30 nm + Trastuzufab (with TA)	iv	2 mg (mice)	Trastuzufab antibody binds to HER2 expressed on tumor cells	BT-474 breast cancer cells	100-200 mm^3 0.2 g	7% (without TA) 15% (with TA)	1.4% (without TA) 3% (with TA)	Dong 2015
IONP of 100 nm (without TA) IONP of 100 nm + Trastuzufab (with TA)	iv	2 mg (mice)	Trastuzufab antibody binds to HER2 expressed on tumor cells	BT-474 breast cancer cells	100-200 mm^3 0.2 g	0.75-1.25% (without TA) 0.75-1.25% (with TA)	0.15-0.25% (without TA) 0.15-025% (with TA)	Dong 2015
IONP (without TA) IONP + Ffab (with TA) IONP + CMD + Ffab (with TA + CMD)	ip	0.75 mg (mice)	Ffab binds to recombinant FOLRα (rFOLRα)	KB cells (human squamous cell carcinoma of the oral cavity)	NA	NA	0% (without TA) 4% (with TA) 7% (with TA + CMD)	Ndong2015
SPION + human serum albumin (with TA)	iv	0.12 mg (mice)	HAS may interact with gp60 and SPARC and yield improved extravasation and tumor accumulation	4T1 breast tumor	500 mm^3 0.6 g	2% (with TA)	1.2% (with TA)	Quan2011
SPION + RGD (with TA)	iv	0.2 mg (mice)	Targets $\alpha_v\beta_3$ integrin-expressing U87MG cells	Glioblastoma U87-MG	180 mm^3 0.2 g	2.6-5.4% (with TA)	0.6-1.2% (with TA)	Yang2011
SPION + PEG (without TA) SPION + PEG + Trastuzumab (with TA)	iv	0.5 mg (mice)	Trastuzufab antibody binds to HER2 expressed on tumor cells	SkBr3 breast cancer cells	65 mm^3 0.1 g	0% (without TA) 8.8% (with TA)	0% (without TA) 0.9% (with TA)	Zolata2015

Table 4

1001

Magnetic targeting of tumors with different types of iron oxyde nanoparticle

IONP type	Admin. Route	Quantity Admin. (animal)	Strength of magnetic field (with MT)	Type of targeted tumor	Tumor size Tumor weight	Percentage of IONP in tumor (% ID/g tissue)	Percentage of IONP in tumor (% ID)	Ref.
SPION encapsulated in nanocapsule	iv	2 mg (mice)	0.43 T	CT-26 colon tumor	100 mm^3 0.2 g	6% (with MT) 2% (without MT)	0.6% (with MT) 0.2% (without MT)	Al-Jamal2016
G100 starch coated IONP (Chemicell)	iv	1.7 mg (rats)	0.4 T	9L glioma	50-70 mm^3 0.1 g	5.10^{-2} % (with MT) 5.10^{-3} % (without MT)	5.10^{-3} % (with MT) 5.10^{-4} % (without MT)	Chertok2007
G-PEI starch coated IONP (zeta potential = 37 mV, Chemicell)	ia	1.7 mg (rats)	0.35 T	9L glioma	70-90 mm^3 0.2 g	0.34 % (with MT)	0.068 % (with MT)	Chertok2010
G-100 starch coated IONP (Zeta potential = -12 mV, Chemicell)	ia	1.7 mg (rats)	0.35 T	9L glioma	70-90 mm^3 0.2 g	0.08%(with MT)	0.16% (with MT)	Chertok2010
SPION (6-10 nm) (Taiwan advanced Nanotech)	iv	0.3 mg (rats)	0.5 T	C6 glioma	20 mm^3 0.1 g	5% (with MT + FUS) 2% (with MT) 1 % (without MT)	0.5% (with MT + FUS) 0.2% (with MT) 0.1 % (without MT)	Fan2013
SPION with amino groups (36 nm)	iv	4 mg (rats)	0.5 T	C6 glioma	23 mm^3 0.1 g	0.5-0.8% (with MT) 0.1% (without MT)	0.05-0.08% (with MT) 0.01% (without MT)	Fan2016
SPION embedded nanobubbles	iv	3 mg (rats)	1.2 T	Glioma tumor	100 mm^3 0.2 g	7% (with MT) 3% (without MT)	1.4% (with MT) 0.6% (without MT)	Huang2013
SPION (ZnMnFeO)	iv	0.8 mg (mice)	Neodinium magnet	4T1 tumor	150 mm^3 0.2 g	12% (with MT) 5% (without MT)	2.4% (with MT) 1% (without MT)	Ni2018
$MoS_2Fe_3O_4$	iv	0.4 mg (mice)	N.A.	PANC-1 (pancreatic tumor)	100 mm^3 0.2 g	4% (with MT)	0.8% (with MT)	Yu2015
Starch coated D-MNP (Chemicell) conjugated with PEG and β-glucosidase	iv	0.24 mg (mice)	0.32 T	9L glioma	300-400 mm^3 0.4 g	6.5% (with MT) 1% (without MT)	2.6% (with MT) 0.4% (without MT)	Zhou2014
Starch coated D-MNP (Chemicell) conjugated with β-glucosidase	iv	0.24 mg (mice)	0.32 T	9L glioma	300-400 mm^3 0.4 g	3% (with MT) 0.5% (without MT)	1.2% (with MT) 0.2% (without MT)	Zhou2014
Starch coated D-MNP (Chemicell)	iv	0.24 mg (mice)	0.32 T	9L glioma	300-400 mm^3 0.4 g	1% (with MT) 0.1% (without MT)	0.4% (with MT) 0.04% (without MT)	Zhou2014

Table 5